# Recent Advances and Perspectives of High-Entropy Alloys as Electrocatalysts for Metal-Air Batteries

Zhang, Xueping; Liu, Yunjian; Zhao, Xiaohua; Cheng, Zhu; Mu, Xiaowei

**Important note**
To cite this publication, please use the final published version (if applicable).
Please check the document version above.

# Recent Advances and Perspectives of High-Entropy Alloys as Electrocatalysts for Metal-Air Batteries

Published as part of Energy & Fuels special issue "2024 Pioneers in Energy Research: Haoshen Zhou".

Xueping Zhang, Yunjian Liu, Xiaohua Zhao, Zhu Cheng,* and Xiaowei Mu*

Read Online

ACCESS | Metrics & More | Article Recommendations

**ABSTRACT:** Metal-air batteries, especially the Li-air and Zn-air ones, have garnered extensive attention and research efforts due to their high theoretical specific energy, safety, and environmental friendliness. Nevertheless, the sluggish kinetics of the cathodes is one of the key factors hindering their practical electrochemical performance. To address this issue, utilizing high-efficiency catalysts is a feasible and effective strategy. Among the varieties of catalysts reported, high-entropy alloys (HEAs) have emerged as a kind of promising catalyst due to their tunable composition and electronic structure. As a result, inspiring battery performances have been achieved in HEAs-catalyzed systems. In this review, we first summarize the reaction mechanism and challenges of the representative metal-air batteries, including Li-$O_2$, Li-$CO_2$, and Zn-air batteries, and then introduce the synthesis methods and core effects of HEAs. We also summarize some research progress on HEAs in these batteries. Finally, we offer insights into the future research prospects of HEAs in metal-air batteries.
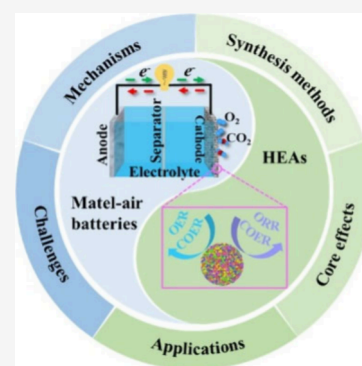
## 1. INTRODUCTION

As industrialization progresses and living standards are elevated, the demand for energy has grown increasingly urgent and significant. The incessant utilization of traditional fossil fuels, such as coal, oil, and natural gas, not only rapidly diminishes their finite reserves but also poses a grave threat to our environment, exacerbating global warming and environmental pollution. Consequently, the exploration and utilization of renewable energy sources stand as the pivotal direction for the future of energy development, offering a sustainable and environmentally friendly alternative. However, renewable energy sources like wind and solar power, which exhibit dispatchable energy generation and intermittent supply characteristics, are challenging to be utilized effectively. Hence, there is a critical need for developing large-scale energy storage systems to facilitate the consistent and stable output of renewable energy sources, thereby ensuring a reliable and sustainable energy supply. Among the various energy technologies, electrochemical energy storage emerges as one of the flexible and more efficient options.[1,2] Notably, rechargeable metal-air batteries stand out as a particularly promising candidate owing to their exceptional theoretical specific energy and environmentally benign properties.[3,4] For instance, the state-of-the-art Li-$O_2$ battery has a remarkable theoretical specific energy of up to 3500 Wh kg$^{-1}$ based on the interaction between Li and $O_2$ to form $Li_2O_2$. Consequently, rechargeable metal-air batteries are widely regarded as the most promising candidates for energy storage systems and have garnered

significant research attention and investigation. However, current advanced metal-air batteries are still facing several challenges, such as the low practical capacity and densities, the low energy conversion efficiency, and the poor cycle life.[5] These issues are closely connected with the sluggish kinetic of $O_2$ reduction reaction (ORR) and $O_2$ evolution reaction (OER) involving multielectron transfers at solid−liquid−gas multiphase interfaces on the air cathode side. Besides, metal dendrites formation and side reactions like the decomposition of electrolyte and carbon cathodes can also cause performance degradation of metal-air batteries.[6−9]

Researchers have made efforts in developing highly efficient catalysts for promoting kinetic of ORR/OER in metal-air batteries, such as carbon-based, noble metal-based, and nonprecious metal-based catalysts.[10−16] Additionally, some studies have been conducted on anode protection strategies and electrolyte modifications to further optimize the performance of metal-air batteries.[17−21] Despite some advancements, the sluggish kinetics of ORR/OER on the cathode side remains a formidable challenge, hindering the attainment of satisfactory electrochemical performance in metal-air bat-

**Figure 1.** Theoretical specific energies and thermodynamic equilibrium potentials of nonaqueous electrolyte-based metal (Li, Na, K)-$O_2$/$CO_2$ batteries and aqueous electrolyte-based metal (Zn, Mg, Al, and Fe)-air batteries. Specific energy densities are calculated based on total weight of the discharge products.

teries.[22] Consequently, there is a critical requirement for the development of innovative and high-activity catalysts that can significantly improve the reaction kinetics on cathodes, thereby improving the performance of metal-air batteries. Furthermore, the semiopen configuration of metal-air batteries poses a unique challenge. Most ORR products can readily react with atmospheric $CO_2$ and generate carbonates that are difficult to decompose. Hence, to prompt the practical application of metal-air batteries, research on metal-$CO_2$ batteries has also been conducted. Resembling metal-$O_2$ batteries, the reactions within metal-$CO_2$ batteries also occur at the multiphase interface involving multielectron transfer processes but using $CO_2$ instead of $O_2$ as the initial active material, resulting in the severe kinetic hysteresis and ultimate degradation of battery performance.

To promote the electrochemical performance of metal-air battery reactions, a prevalent approach involves employing catalysts to accelerate the reaction kinetics and lower the overpotentials. The ideal catalysts should embody the following quintessential characteristics: (1) good electronic conductivity to facilitate charge transfer and minimize interfacial resistance; (2) large surface area to provide more space for electrochemical reactions; (3) porous structure for gas and electrolyte diffusion as well as storage space for discharge products; (4) excellent intrinsic catalytic activity; and (5) good structural stability. In recent years, the emergence of high-entropy alloys (HEAs) with remarkable electronic structure and properties have attracted significant interest from researchers.[23−26] Apart from their commendable electronic conductivity, HEAs exhibit four core effects: high-entropy effect, lattice distortion effect, sluggish diffusion effect, and cocktail effect. Notably, lattice distortion contributes to the formation of defects and strains in HEAs. Previous studies have indicated that lattice defects can modulate the electronic structure and thus affect the interaction of the active sites with the reactants.[27] In other words, lattice defects can significantly optimize the catalytic activity of materials.[28,29] Additionally, the cocktail effect, characterized by the synergistic interplay of multiple metallic elements, further improves the catalytic

performance of HEAs.[30] Moreover, the sluggish diffusion effect contributes to the remarkable structural stability of HEAs, making them highly promising for electrocatalysis applications. In the past few years, over a hundred reviews have been made in the study of HEAs electrocatalysis. However, there are a few reviews focused on their application in the energy storage field, especially in the context of metal-air batteries that involve the performance of Li-$O_2$ batteries and Zn-air batteries. Moreover, investigations of Li-$CO_2$ batteries were also carried out. Therefore, to better promote the research and development of HEAs in the field of metal-air batteries, it is necessary to summarize the research advancements on HEAs as catalysts for metal-air batteries.

In this review, we first summarize the mechanisms and challenges of metal-air batteries, followed by an overview of the synthesis methods employed for HEAs and their properties. Subsequently, we showcase several exemplary HEAs that have demonstrated promising applications in three common metal-air battery systems: Li-$O_2$ batteries, Li-$CO_2$ batteries, and Zn-air batteries. Finally, we offer insightful perspectives on the future development of HEAs in terms of compositional optimization, advanced characterization techniques, and broadened application scopes within metal-air batteries.

## 2. BRIEF OVERVIEW OF RECHARGEABLE METAL-AIR BATTERIES

Metal-air batteries usually consist of metal anodes, electrolytes, and porous cathodes. According to the type of electrolyte, they can be categorized into two groups. One group is nonaqueous electrolyte-based batteries, including Li-air batteries, Na-air batteries, and K-air batteries. Given their operation in dry, pure $O_2$ or $CO_2$ environments, these are more precisely termed metal-$O_2$ or metal-$CO_2$ batteries, exemplified by Li-$O_2$ and Li-$CO_2$ batteries. The other group is aqueous electrolyte-based metal-air batteries, which can work directly in air, such as Zn-air batteries, Al-air batteries, Mg-air batteries, and Fe-air batteries. Figure 1 provides a comparative analysis of the theoretical specific energies and thermodynamic equilibrium

voltages across various cell types, including nonaqueous and aqueous systems.[31−33] The Li-$O_2$ battery has a remarkable thermodynamic equilibrium potential of 2.96 V and an exceptional theoretical energy density of 3500 Wh kg$^{-1}$, which surpasses the state-of-the-art lithium-ion batteries by a factor of 5 to 10 times.[34] Similarly, other metal-air battery systems also exhibit specific energies exceeding those of lithium-ion batteries. Among these battery systems, Li-$O_2$ batteries, Li-$CO_2$ batteries, and Zn-air batteries have garnered significant research attention, being the most extensively studied members of the metal-air battery family.

However, studies of rechargeable metal-air batteries remain in the early stages, with their realized energy densities lagging significantly behind their theoretical potential. Furthermore, they suffer from relatively low power densities and poor cycle performance, posing challenges in meeting practical demands. One pivotal factor contributing to the above issues lies in the sluggish kinetics of ORR/OER or the $CO_2$ reduction and evolution reactions ($CO_2RR/CO_2ER$) occurring at the cathodes. To address this issue at its core, a profound understanding of the reaction mechanisms underlying metal-air batteries is imperative. In this section, we provide a comprehensive summary of the reaction mechanisms pertaining to Li-$O_2$ batteries, Li-$CO_2$ batteries, and Zn-air batteries.

**2.1. The Reaction Mechanism of Li-$O_2$ Batteries.** The reaction of a Li-$O_2$ battery is a complex electrochemical reaction that occurs at the triple-phase interface between the catalyst (solid)-electrolyte (liquid)-$O_2$ (gas).[35] The mechanism of $O_2$ reduction to form $Li_2O_2$ during the discharge process is illustrated in Figure 2a.[32,36] On the anode side, the metal Li
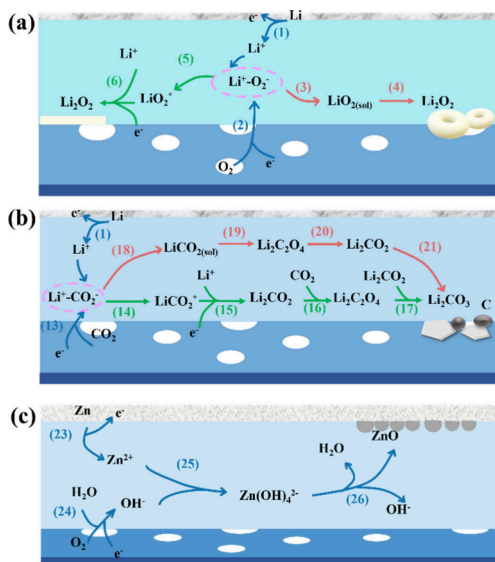


**Figure 2.** Schematic diagrams illustrating mechanisms of the (a) Li-$O_2$ battery, (b) Li-$CO_2$ battery, and (c) Zn-air battery during the discharge process.

loses an electron and becomes Li$^+$ (as described in eq 1) that diffuses into the electrolyte. For the $O_2$ cathode side, $O_2$ is absorbed on the surface of the $O_2$ host material (usually porous carbon) and obtains electrons from the external circuit via a reduction reaction to generate $O_2^-$ (as described in eq 2), and then $O_2^-$ combines with Li$^+$ to form the intermediate product Li$^+$-$O_2^-$:

$$Li \rightarrow Li^+ + e^- \tag{1}$$

$$Li^+ + O_2 + e^- \rightarrow Li^+ - O_2^- \tag{2}$$
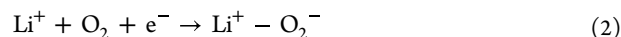
The discharge process of the Li-$O_2$ battery is influenced by the location of the discharge intermediates $LiO_2$. Whether $LiO_2$ is adsorbed on the electrode surface or dissolved in the electrolyte is determined by factors such as the electrolyte solvent, the electrode surface adsorption strength, the electrode potential, and the discharge current.[32,37] Depending on the location of $LiO_2$, here are two possible pathways for the formation of the final discharge product $Li_2O_2$ from Li$^+$-$O_2^-$: the solution pathway and the surface pathway. For the solution pathway, eq 3 occurs, and the generated $LiO_2$ dissolves into the electrolyte. Subsequently, a disproportionation reaction of $LiO_2$ takes place, resulting in the formation of relatively large toroidal $Li_2O_2$ and gaseous $O_2$ (as described in eq 4). This disproportionation reaction leads to the breakage of the O−O bond, resulting in the formation of partially singlet oxygen ($^1O_2$). The highly reactive singlet oxygen is a critical factor in inducing the chain decomposition of the electrolyte, which accelerated battery aging:[38]

$$Li^+ - O_2^- \rightarrow LiO_{2(sol)} \tag{3}$$

$$2LiO_{2(sol)} \rightarrow Li_2O_2 + O_2/^1O_2 \tag{4}$$
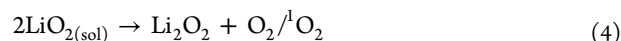
For the surface pathway: $LiO_2$* is deposited on the surface of the electrode by eq 5, and a one-step electrochemical reaction occurs after eq 6 to form film-like $Li_2O_2$:

$$Li^+ - O_2^- \rightarrow LiO_2^* \tag{5}$$

$$LiO_2^* + Li^+ + e^- \rightarrow Li_2O_2 \tag{6}$$
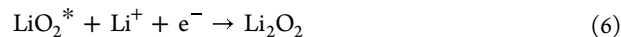
During the charging process, decomposition of $Li_2O_2$ occurs. However, due to its wide band gap of approximately 4−5 eV, $Li_2O_2$ requires a significant charging overpotential to decompose.[39,40] As a result, researchers are actively working on developing high-performance catalysts that can effectively reduce the charging overpotential of Li-$O_2$ batteries. Initially, $Li_2O_2$ undergoes partial delithiation, forming $Li_{2-x}O_2$ as described by eq 7:

$$Li_2O_2 \rightarrow Li_{2-x}O_2 + xLi^+ + xe^- \tag{7}$$
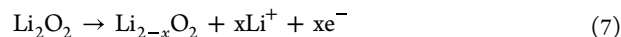
The subsequent reactions in the charging process are analogous to those in the discharge process with both the solution pathway and the surface pathway being involved. $Li_{2-x}O_2$ continues to decompose into $LiO_{2(sol)}$ and Li$^+$ (as described by eq 8), which might be followed by the disproportionation of $LiO_{2(sol)}$ into $Li_2O_2$ and $O_2$ (as described by eq 9). Eqs 7−9 steps together are referred to as the solution pathway:

$$Li_{2-x}O_2 \rightarrow LiO_{2(sol)} + (1-x)Li^+ + (1-x)e^- \tag{8}$$

$$2LiO_{2(sol)} \rightarrow Li_2O_2 + O_2 \tag{9}$$
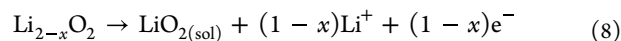
Through the surface pathway, $Li_{2-x}O_2$ directly decomposes into Li$^+$ and $O_2$ (as described by eq 10). These are the two primary decomposition pathways of $Li_2O_2$. In summary, eq 11 represents the overall reaction of a Li-$O_2$ battery:

$$Li_{2-x}O_2 \rightarrow O_2 + Li^+ \tag{10}$$

$$\text{Overall reaction: } 2Li + O_2 \leftrightarrow Li_2O_2 \tag{11}$$
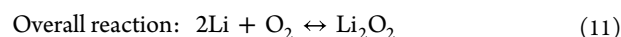
## 2.2. The Reaction Mechanism of Li-CO$_2$ Batteries.

Similar to Li-O$_2$ batteries, Li-CO$_2$ batteries also involve reactions at the triple-phase interface. In general, it is considered that rechargeable Li-CO$_2$ batteries undergo the overall discharge reaction (eq 12):[41,42]

$$4Li + 3CO_2 \rightarrow 2Li_2CO_3 + C \tag{12}$$
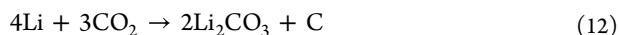
Figure 2b shows the reaction steps during the discharge process of a Li-CO$_2$ battery. At the anode, Li loses an electron and becomes Li$^+$ diffusing into the electrolyte. CO$_2$ molecules are adsorbed on the catalyst active sites on the cathode surface. The absorbed CO$_2$ molecule can capture an electron and is reduced to the CO$_2^-$ species by eq 13. Subsequently, CO$_2^-$ combines with Li$^+$ to form LiCO$_2$ (eq 14). Given the solubility of LiCO$_2$ in the electrolyte or the adsorption energy at the cathode surface, the formation of Li$_2$CO$_3$ also involves two reaction pathways: the solution pathway and the surface pathway. If LiCO$_2$ is absorbed on the electrode surface, then it further combines with Li$^+$ and an electron to generate Li$_2$CO$_2$ (eq 15). Then Li$_2$CO$_2$ reacts with the absorbed CO$_2$ to form Li$_2$C$_2$O$_4$ (eq 16), which combines with Li$_2$CO$_2$ to eventually form the discharge product Li$_2$CO$_3$ and C (eq 17). The above processes are the mechanism of Li$_2$CO$_3$ formation via the surface pathway:

$$CO_2 + e^- \rightarrow CO_2^- \tag{13}$$

$$Li^+ - CO_2^- \rightarrow LiCO_2^* \tag{14}$$

$$Li^+ + LiCO_2^* + e^- \rightarrow Li_2CO_2 \tag{15}$$

$$CO_2 + Li_2CO_2 \leftrightarrow Li_2C_2O_4 \tag{16}$$

$$Li_2C_2O_4 + Li_2CO_2 \rightarrow Li_2CO_3 + C \tag{17}$$
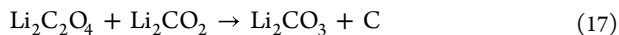
If LiCO$_2$ dissolves easily in the electrolyte, LiCO$_{2(sol)}$ forms by eq 18, and two LiCO$_{2(sol)}$ molecules first combine to generate Li$_2$C$_2$O$_4$ (eq 19). Then the disproportionation reaction of two Li$_2$C$_2$O$_4$ occurs to form Li$_2$CO$_2$ and CO$_2$ (eq 20). Finally, the discharge products Li$_2$CO$_3$ and C are formed through the reaction between Li$_2$C$_2$O$_4$ and Li$_2$CO$_2$ (eq 21):

$$Li^+ - CO_2^- \rightarrow LiCO_{2(sol)} \tag{18}$$

$$2LiCO_{2(sol)} \rightarrow Li_2C_2O_4 \tag{19}$$

$$Li_2C_2O_4 \rightarrow Li_2CO_2 + CO_2 \tag{20}$$

$$Li_2C_2O_4 + Li_2CO_2 \rightarrow Li_2CO_3 + C \tag{21}$$
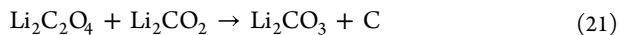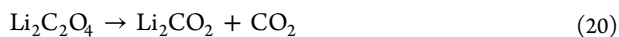
In addition to the case where the discharge product generates Li$_2$CO$_3$ and C, there is also a case where the discharge product is stable Li$_2$C$_2$O$_4$. It is generally realized using specific solid catalysts (Mo-based catalysts) or liquid catalysts (also be known as redox mediator, RM),[43−47] which case we will not discuss here.

In the charging process of Li-CO$_2$ batteries, the decomposition of Li$_2$CO$_3$ occurs. The decomposition of Li$_2$CO$_3$ with a wide-bandgap requires a larger charging overpotential, leading to a low energy efficiency and poor cycling performance. Studies in recent years have found that the decomposition of Li$_2$CO$_3$ has one reversible pathway and two irreversible pathways. The evolution of CO$_2$ accompanies with the generation of byproducts, like $^1O_2$ and $O_2^{\bullet-}$ via the irreversible pathways, as displayed in eqs 22 and 23, respectively:[48−50]

$$2Li_2CO_3 \rightarrow 2CO_2 + {}^1O_2 + 4Li^+ + 3e^- \tag{22}$$

$$2Li_2CO_3 \rightarrow 2CO_2 + O_2^{\bullet-} + 4Li^+ + 3e^- \tag{23}$$
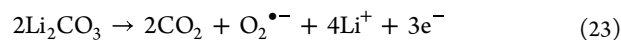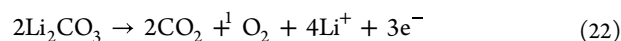
To realize efficient energy conversion, researchers prefer the reversible reaction of eq 12 to occur within Li-CO$_2$ batteries. In this case, the reversible pathway of the Li$_2$CO$_3$ decomposition is shown in eq 24:[41,51,52]

$$2Li_2CO_3 + C \rightarrow 4Li^+ + 3CO_2 + 4e^- \tag{24}$$

## 2.3. The Reaction Mechanism of Zn-Air Batteries.

Primary Zn-air batteries are now commercially available and have been successfully used in medical and telecommunication applications, such as hearing aids and wireless messaging devices.[53,54] In recent years, rechargeable Zn-air batteries have gained revived interests as one kind of next-generation electrochemical energy storages because of their high theoretical energy densities, wide operational temperature range, low cost, zero pollution, and high safety.[55,56] In order to develop high-performance Zn-air batteries, it is vital to understand their reaction mechanisms.

During the discharge process of the battery, the anode metal Zn loses electrons and is oxidized to Zn$^{2+}$ (eq 25).[57,58] The oxygen on the cathode surface generates electrons to generate OH$^-$ (eq 26), which combines with Zn$^{2+}$ in the electrolyte to produce soluble $[Zn(OH)_4]^{2-}$ (eq 27). Afterward, $[Zn(OH)_4]^{2-}$ converts into insoluble ZnO when $[Zn(OH)_4]^{2-}$ is supersaturated in solution through eq 28. It is important to point out that the discharge product ZnO is deposited on the surface of the anode instead of inside the porous cathode commonly seen in Li-O$_2$ and Li-CO$_2$ batteries:

$$Zn \rightarrow Zn^{2+} + 2e^- \tag{25}$$

$$O_2 + 4e^- + 2H_2O \rightarrow 4OH^- \tag{26}$$

$$Zn^{2+} + 4OH^- \rightarrow [Zn(OH)_4]^{2-} \tag{27}$$

$$[Zn(OH)_4]^{2-} \rightarrow ZnO + H_2O + 2OH^- \tag{28}$$
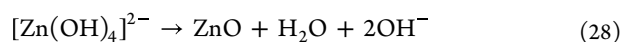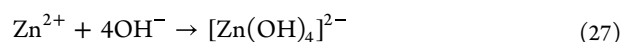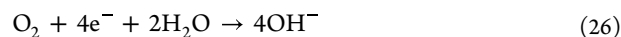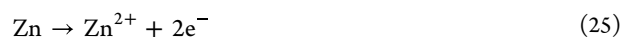
In the rechargeable Zn-air battery, reduction reaction of Zn$^{2+}$ occurs on the anode side during the charging process.[59] First, ZnO and OH$^-$ combine with H$_2$O to produce $[Zn(OH)_4]^{2-}$ (eq 29), followed by the reduction of $[Zn(OH)_4]^{2-}$ to Zn (eq 30). At the cathode side, OH$^-$ undergoes oxidation to produce O$_2$ (eq 31), which is also an OER process. The overall reaction of rechargeable Zn-air batteries is depicted in eq 32:

$$ZnO + H_2O + 2OH^- \rightarrow [Zn(OH)_4]^{2-} \tag{29}$$

$$[Zn(OH)_4]^{2-} + 2e^- \rightarrow Zn + 4OH^- \tag{30}$$

$$2OH^- \rightarrow 1/2O_2 + H_2O + 2e^- \tag{31}$$

$$Overall\ reaction:\ 2Zn + O_2 \leftrightarrow 2ZnO \tag{32}$$
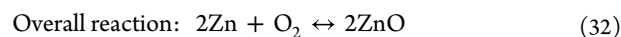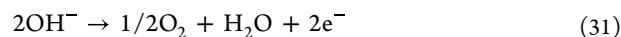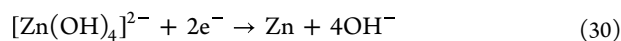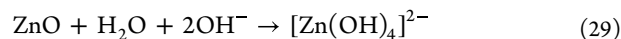
Based on the reaction steps outlined above, it is evident that the discharge−charge process of a rechargeable Zn-air battery is achieved through water-involved ORR/OER processes. Therefore, enhancing the kinetics of the ORR/OER processes, which are analogous to the half-reactions in water electrolysis, can lead to improved performance of Zn-air batteries.

**2.4. Challenges of Rechargeable Metal-Air Batteries.** There are still several noticeable obstacles that hinder the practical application of metal-air batteries. First, the intricate multistep electron transfer process inherent in all metal-air batteries gives rise to sluggish kinetics in ORR/OER reactions. Specifically, in $Li$-$O_2$ and $Li$-$CO_2$ batteries, the discharge byproducts $Li_2O_2$ and $Li_2CO_3$, both being electronic insulators, accumulating on electrode surfaces, exacerbate reaction resistance during subsequent discharge cycles. This phenomenon significantly increases the overpotential required for $ORR/CO_2RR$ processes. Additionally, the sluggish decomposition kinetics of $Li_2O_2$ and $Li_2CO_3$ during charging further contributes to huge overpotentials in the $OER/CO_2ER$ processes, thereby diminishing the overall energy conversion efficiency of these batteries. Second, the emergence of metal dendrites constitutes a formidable challenge to the stability of metal-air batteries. Over prolonged cycling, uneven metal deposition leads to the growth of Li or Zn dendrites, which can potentially penetrate the separator, triggering short-circuits and significant capacity fade. In the case of Zn-air batteries, additional concerns arise from hydrogen evolution and Zn corrosion, which are non-negligible issues that further complicate their operational reliability. Lastly, yet importantly, the instability of electrolytes represents a pivotal issue that significantly impacts the long-term performance of batteries. For $Li$-$O_2$ batteries and $Li$-$CO_2$ batteries, electrolyte degradation can occur through spontaneous decomposition as well as through attack by highly reactive intermediates generated during cycling. This degradation not only undermines the overall stability of the batteries but also compromises their operational efficiency and lifespan. Jiang et al. improved the performance of $Li$-$O_2$ batteries using a strategy involving singlet oxygen quenchers.[60]

To tackle the issue of kinetic hysteresis in ORR/OER or $CO_2RR/CO_2ER$ in metal-air batteries, researchers have utilized carbon materials with large specific surface area and high conductivity, such as carbon nanotubes and graphene, as cathode catalysts for metal-air batteries. However, the reported carbon catalytic activity is still unsatisfactory for OER, and there are many other issues such as degradation of carbon.[61] Alternatively, noble metals and transition metals are commonly employed as catalysts in metal-air batteries. Noble metals exhibit comprehensive catalytic activities, but selectivity favors certain reactions over others. Moreover, their high costs impede their large-scale development and application in metal-air batteries. Transition metal catalysts, when compared to precious metals, often exhibit inferior catalytic activity, prompting researchers to embark on a quest for cost-effective alternatives with enhanced catalytic performance for metal-air batteries.[62−67] Recently, HEAs have emerged as a promising new frontier, attracting considerable attention due to their exceptional properties, including wide d-band centers, tunable electronic structures, remarkable stability, and cost-effectiveness. These unique properties of HEAs offer many opportunities to tackle the challenges of sluggish kinetics in ORR/OER and $CO_2RR/CO_2ER$, as well as issues related to catalyst structural instability and high costs.

# 3. HIGH-ENTROPY ALLOYS

**3.1. Definition of HEAs.** Entropy is a function of the thermodynamic state of a system, which represents the degree of chaos of the system by the Boltzmann's hypothesis.[68] The entropy of the macroscopic state of the system is proportional to the number of microstates corresponding to the macroscopic state of the system. The equation is as follows:

$$\Delta S_{mix} = -R[c_1 \ln c_1 + c_2 \ln c_2 + \cdots + c_n \ln c_n]$$
$$= -R \sum_{i=1}^{n} c_i \ln c_i \qquad (33)$$

where $S$ is the entropy, $R$ is the gas constant, $c_i$ is the atomic percentage of each component, and $n$ is the total number of the components. If the alloy material contains the same amount of each element, the formula can be simplified to the following equation:

$$\Delta S_{mix} = R \ln n \qquad (34)$$

When the values of $\Delta S_{mix}$ are greater than 1.5R, alloys are HEAs. If $1R \leq \Delta S_{mix} \leq 1.5R$, the materials are medium-entropy alloys. When the values of $\Delta S_{mix}$ are smaller than 1R, alloys are low-entropy alloys.

HEAs are composed of 5 or more major elements, and the atomic fraction of each major element >5% and <35%. In recent years, with the research and exploration of HEAs, their definitions have become more and more broad. From the perspective of composition, new alloys that now contain four or more constituent elements, with the elements composed according to the nonequal atomic ratio, and no element content exceeding 50%, can be defined as HEAs.

**3.2. Synthesis Methods of HEAs.** In Figure 3, we provide a comprehensive overview of the various preparation methods
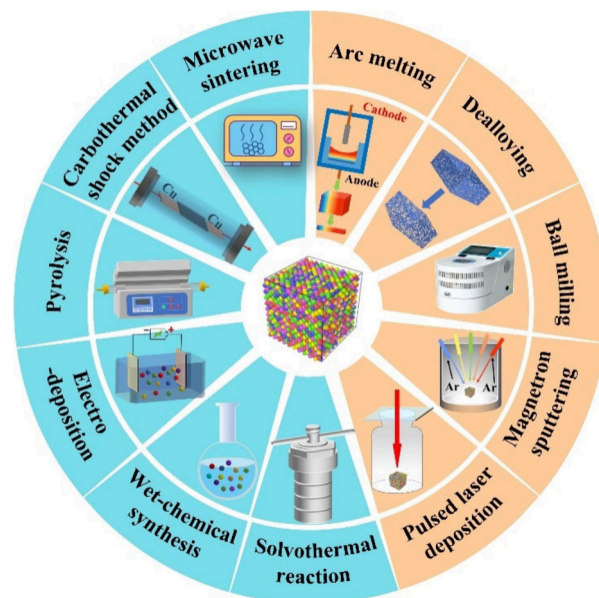


**Figure 3.** Schematic illustration of the synthesis methods of HEAs. These synthetic methods can be classified into two main groups according to their raw materials and preparation mechanisms. The top-down strategies are shown in the orange region and the bottom-up strategies are shown in the blue region.

employed for the synthesis of HEAs, offering a clear and concise summary of the techniques. There are two primary strategies for synthesizing HEAs: the top-down strategy, which involves breaking down bulk material (orange zone), and the bottom-up strategy, which involves reducing metal salt precursors (blue zone).

*3.2.1. The Top-down Approaches.* The top-down approach refers to the physical method of preparing HEAs by crushing large blocks of materials. Here, we summarize five top-down approaches for synthesizing HEAs.

*3.2.1.1. Vacuum Melting Technology.* Vacuum melting technology is a conventional method for preparing HEAs, involving arc-melting and induction melting. All alloy ingots are created by smelting samples in an Ar atmosphere, ensuring a uniform composition through magnetic stirring. The ingots are then placed into a mold and cut using wire cut machining to form a suitable sheet.[69,70] This approach is commonly utilized in traditional metal materials research. It is ideal for metals with high melting points, yielding high purity alloys. Nonetheless, the method is costly, and the resulting alloys are typically in the block form with a limited specific surface area.

*3.2.1.2. Dealloying Method.* Dealloying method is a technique used to selectively eliminate or reduce the remaining components of one or more active components by leveraging the chemical activity difference between different components in the alloy through a chemical or electrochemical process.[71,72] This process allows for the creation of porous alloy materials through atomic diffusion and aggregation. While this method is frequently utilized for designing and preparing porous alloy materials, it requires obtaining the alloy sheet or ball first through other methods, such as arc-melting. Jin et al. utilized a dealloying method to prepare highly dispersed PtPdCuAgAu HEA clusters loaded on high-entropy metal oxide substrates as bifunctional catalysts for metal-air batteries.[73]

*3.2.1.3. High-Energy Ball Mill Method.* The ball milling method, also known as mechanical alloying, involves using powder in a high-energy ball mill and grinding ball to induce prolonged impact, collision, repeated cold welding, and fracture processes. HEAs are formed through the diffusion of atoms in the powder particles.[74] This method is often combined with sintering and melting techniques to prepare HEAs.

*3.2.1.4. Magnetron Sputtering Method.* Magnetron sputtering is a method of physical vapor deposition that utilizes ionized Ar to excite each metal target, ionize metal ions, and deposit them on the substrate to form HEA clusters or films.[75,76] This technique offers benefits such as low film-forming temperature, dense film layers, and strong adhesion. It is commonly employed in the production of HEAs films or clusters, although it may pose challenges in the formation of dispersed particles.

*3.2.1.5. Pulsed Laser Deposition Method.* Pulsed laser deposition can be used to prepare the HEAs particles. The laser is focused on small areas of multiple metal targets, using high energy to partially evaporate or ionize the target materials. Then, the metal ions are deposited on the substrate, forming particles.[77] While this method is rapid and efficient, it may not be suitable for producing large quantities of particles.

*3.2.2. The Bottom-up Approaches.* The bottom-up approach primarily refers to the method of obtaining HEAs by reducing metal salt precursors, which are obtained through chemical reactions, such as solvothermal synthesis. Below, we describe six bottom-up approaches for preparing HEAs.

*3.2.2.1. Solvothermal Synthesis.* The solvothermal synthesis method is a conventional wet chemistry approach for preparing alloys. Various metal salts are dispersed in water or alcohol solutions and heated at a lower temperature for reduction to obtain HEA nanoparticles on the substrate.[78] This method is straightforward, energy-efficient, and suitable for the

batch preparation of particles. However, controlling the synthesis process can be challenging, leading to issues, such as particle agglomeration and oxidation. PtIrPdRhRu nanoparticles were obtained by the simple and benign solvothermal synthesis method.[79]

*3.2.2.2. Low-Temperature Oil-Phase Processing.* Similar to the solvothermal synthesis method, low-temperature oil-phase processing is a wet chemistry technique. Metal salts are mixed in illuminating or other solvents, heated to a suitable temperature, and maintained for a specific time. HEAs were obtained after washing times and placing in a vacuum drying oven for drying.[80,81] This method operates at low synthesis temperatures, resulting in uniform alloy particle sizes. It is a simple and energy-efficient approach but may not be suitable for insoluble metal salts. Sun et al. synthesized a series of HEA nanowires via a low-temperature oil phase method.[82]

*3.2.2.3. Electrodeposition Processing.* A clean substrate (iron sheet, nickel foam, etc.) is prepared and the required ratio of metal salt solution containing a complexing agent. Then the electrodeposition process is carried out using a potentiated three-electrode system in the above solution. The three-electrode setup consists of the substrate as the working electrode, a Hg/HgO electrode as the reference electrode, and a Pt electrode as the counter electrode. Electrodeposition technology offers ease of use and control at low temperatures, including potentiated, calvinistic, CV, pulse, cathodic plasma, and droplet-mediated electrodeposition methods.[77,83,84] Desired particle size of the HEA can be controlled by adjusting parameters such as solution concentration, deposition current, and deposition time. In comparison to the high-temperature furnace method, it boasts a low energy consumption. Zhang et al. prepared the FeCoNiMnW HEA onto the surfaces of the constituent carbon fibers of a carbon paper via the pulse current electrodeposition method.[85] However, the homogeneity of the alloy phase is influenced by the metal ion deposition potential and the complexing agents. Additionally, this necessitates the deposition of the alloy on a support with electrical conductivity.

*3.2.2.4. Pyrolysis Method.* Pyrolysis is a commonly employed method for preparing HEAs antiparticles. Initially, all metal salt solutions polymerize, followed by pyrolysis and reduction under an Ar/H$_2$ atmosphere at high temperatures. This method is straightforward, allowing for the batch preparation of alloy materials. While it utilizes simple equipment and a well-established synthesis process, challenges exist in achieving rapid heating and cooling.[86] The development of fast-moving bed pyrolysis by Gao et al. has effectively addressed these challenges.[87] This method ensures rapid mixing of metal precursors and simultaneous pyrolysis at high temperatures, leading to the formation of nuclei with a small size.

*3.2.2.5. Carbon Thermal Shock Method.* The carbon thermal shock method is a technique that utilizes joule heat generated by the current to prepare HEAs particles.[88] Metal salt precursors are uniformly mixed with carbon material and exposed to rapid high temperatures and cooling under Ar/H$_2$ conditions. This process results in the formation of homogeneous particles with uniform temperature distribution, fast heating/cooling rates, high reaction temperatures, and ultrafast reaction times. The instantaneous high temperature allows for the pyrolysis of mixed metal salts and the formation of metal droplets simultaneously. The short holding time ensures the proper concentration of metal atoms on the carbon

fiber surface, maintaining a dynamic equilibrium of droplet splitting and fusion behavior to prevent particle growth. This method is effective for synthesizing HEA particles of uniform size quickly and on a large scale, but it is suitable only for conductive supports. In comparison to traditional pyrolysis methods in tubular furnaces, it enhances the preparation efficiency and reduces energy consumption.

*3.2.2.6. Microwave Sintering Method.* Microwave sintering is a method similar to the carbon thermal shock technique. In this approach, metal salt is mixed with a carbon carrier and placed in a microwave environment to obtain a HEA by absorbing a significant amount of energy through the carbon carrier.[89,90] It offers advantages, such as short heating times and high efficiency. Unlike the carbon thermal shock method, this technique necessitates the use of a heat-absorbing carrier material.

Top-down approaches typically involve high pressure, high temperature, and an inert gas environment. Moreover, when bottom-up approaches are used, some factors such as the reduction potential of metals and the compatibility between different elements should be taken into account. Given the unique characteristics of the aforementioned methods for synthesizing HEAs, and taking into account the specific requirements of catalysts for metal-air batteries, it is conceivable that these techniques may hold significant potential for the preparation of nanoscale catalysts tailored for such applications. Unlike the applications of HEAs in other fields, when using HEAs as catalysts, it is essential to take into consideration the intrinsic catalytic abilities of metal elements and the particle size of the HEAs. The design and synthesis of HEAs are constrained by these factors, indicating the need for the development or improvement of their synthesis methods in the future. Specifically, methods such as dealloying, pulsed laser deposition, solvothermal synthesis, low-temperature oil-phase processing, pyrolysis, carbon thermal shock method, and microwave sintering method may produce nanoscale HEA catalysts that exhibit optimal properties for metal-air batteries. However, from a practical perspective, solvothermal synthesis, low-temperature oil-phase processing, pyrolysis, the carbon thermal shock method, and microwave sintering methods are more suitable for preparing HEA catalysts for metal-air batteries. Alongside the stringent synthesis conditions and design outlined above, the stability also necessitates further investigation.

**3.3. Core Effects of HEAs.** Although the preparation methods of HEAs share similarities with those of traditional alloys, they exhibit distinct properties. These differences are closely related to the four core effects of HEAs (Figure 4).

*3.3.1. High-Entropy Effect.* In traditional alloys, a limited number of major elements are typically selected, and their content is adjusted to control the alloy's properties. However, in HEAs, a homogeneous blend of five or more elements is utilized, resulting in a highly disordered atomic structure. This system exhibits a significant mixed entropy, which favors a single-phase solid solution structure.[91] This unique structure enhances the alloy's entropy, leading to improved thermal stability and resistance to deformation. The high-entropy effect endows HEAs with exceptional high-temperature stability and mechanical properties, making them suitable for use in various extreme environments.

*3.3.2. Lattice Distortion Effect.* In HEAs, the presence of neighboring atoms with varying atomic sizes and asymmetric bonds causes each atom to deviate from its average lattice
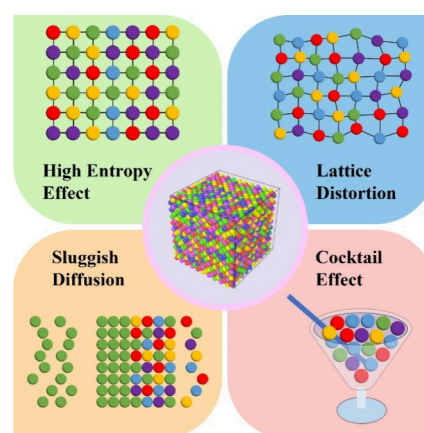


**Figure 4.** Schematic diagram of the four core effects of the HEAs.

position, resulting in significant lattice distortion in the alloy. This distortion leads to a complex crystal structure, including various lattice defects and dislocations. As a result, the lattice parameters of HEAs undergo changes, leading to a reduced intensity of X-ray diffraction peaks.[92] Moreover, these lattice distortions not only enhance the strength and hardness of the alloy but also improve the heat and corrosion resistance. The lattice distortion effect confers outstanding performance on HEAs under a wide range of high stress and high temperature conditions. Additionally, the lattice strain influences the bonding mode and catalytic selectivity with reaction intermediates. Furthermore, lattice distortion in HEAs can facilitate the increase of electron density near the Fermi level ($E_f$) and accelerate the electron transfer rate.

*3.3.3. Slow Diffusion Effect.* The presence of different types and sizes of adjacent atoms in HEAs leads to a uniform distribution of atoms and severe lattice distortion within a unit. Consequently, the diffusion rate of atoms in the lattice becomes very slow and difficult as it becomes more challenging for atoms to follow their jump path in the lattice site, increasing the diffusion activation energy. This slow diffusion effect endows HEAs having better structural stability and excellent oxidation and corrosion resistance properties, making them suitable for applications in various harsh environments. Furthermore, the slow diffusion effect helps to improve the processability of the alloy, making it easier to form and manufacture.

*3.3.4. Cocktail Effect.* The cocktail effect refers to the interaction and competition among various elements in HEAs. Since HEAs contain a wide variety of elements and their proportions are often nearly uniformly distributed, complex interactions between different elements occur. The properties of an HEA are influenced not only by the microstructure resulting from the combination of these elements but also by the individual impact of each element. For instance, if elements with good oxidation resistance, such as Al and Cr, are added, the oxidation resistance of the alloy can be enhanced. Many HEAs utilize precious metal elements with good catalytic activity, such as Ru, Ir, and Pt, to improve their catalytic performance.[93] This interaction between the elements in a HEA not only leads to changes in the microstructure and properties of the alloy but also affects the overall material properties. The cocktail effect offers HEAs a rich variety of microstructures and properties, providing more possibilities for material design and optimization, such as the synergistic effect on catalytic reactions.

**3.4. Application of HEAs.** HEAs, as a kind of novel material, exhibit outstanding physical and mechanical properties, including high-temperature strength, fracture toughness, corrosion resistance, and wear resistance. They are now extensively utilized in the aerospace, automotive manufacturing, and energy industries and emerge as the preferred option for researchers and engineers as functional materials.

As the exploration and study of HEAs progress to the microscale, such as nanoscale particles, their application range has broadened to include the medical, energy storage, and catalysis sectors. Furthermore, recent research findings suggest that HEA nanoscale particles act as effective and durable catalysts, offering numerous active sites for various catalytic reactions like hydrogen reduction reaction (HER), ORR, OER, and $NH_3$ reduction. For the application of HEAs in metal-air batteries, we will expand on HEAs for the ORR/OER and the $CO_2RR/CO_2ER$ in the next section.

# 4. APPLICATIONS OF HEAS FOR RECHARGEABLE METAL-AIR BATTERIES

The cathode-side scientific challenges of metal-air batteries encompass the sluggish kinetics of the ORR/OER processes and the poor conductivity of reaction products, which can lead to the accumulation of oxides/carbonates and subsequent electrode passivation. Noble metals, particularly Pt, have been widely employed as effective catalysts for ORR.[94,95] Meanwhile, Ru, Ir, and their oxides are renowned for their exceptional catalytic properties for OER.[96−98] To enhance the catalytic activity of the ORR/OER and $CO_2RR/CO_2ER$ processes and reduce catalyst costs, researchers have developed bifunctional catalysts by alloying strategies.

HEAs, characterized by wide electronic band gaps and a multitude of localized electronic states, have garnered attention in recent years for their superior catalytic activity and stability compared to conventional alloys. The unique composition and distribution of different atomic elements in HEAs can modulate the position and intensity of the d-band center, thereby influencing the surface adsorption abilities and activation energies of the catalysts. This inherent attribute facilitates a remarkable enhancement in the catalytic performance of HEAs through electronic structure modulation, achieved by adjusting the elemental composition and inducing lattice distortion. Thus, HEAs present novel perspectives and avenues for enhancing the performance of metal-air batteries, offering promising solutions to overcome the limitations associated with traditional catalysts and advancing the field toward more efficient and cost-effective catalytic.

In the next section, we will discuss in detail the relationship between the electronic structure of HEAs, the catalytic activity, and the performance of metal-air batteries.

**4.1. HEAs in Li-O₂ Batteries.** Tao et al. synthesized a series of subnanometer ribbon HEAs (PtPdIrRuAgX, X = Au, Au) with a face-centered cubic (FCC) structure using a galvanic exchange pathway (Figure 5a and b).[99] Li-O₂ batteries utilizing PtPdIrRuAuAg SNRs demonstrated a discharge capacity of 5252 mAh g⁻¹ and a low charge overpotential of 0.87 V at a current density of 0.10 A g⁻¹ (Figure 5c). They demonstrated that when Au was paired with other metals, the density of states of Au in the PtPdIrRuAuAg HEA became more electron-rich. Especially, the reducing ability of the alloy was improved, while the Au-5d orbital was coupled with the Ag-4d orbital. The high local electron densities of Ru, Ir, and Pd in PtPdIrRuAuAg SNRs resulted in a low energy barrier for
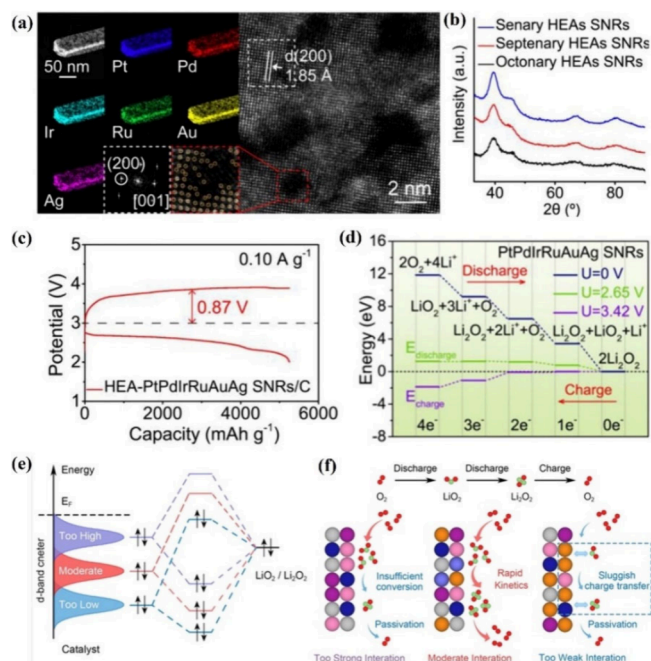


**Figure 5.** (a) HAADF-STEM image, EDS element mapping images, and high-resolution HAADF-STEM image of the HEA-PtPdIrRuAuAg SNR with the corresponding FFT pattern taken from the white dashed area in (a) and the enlarged atomic resolution HAADF-STEM image taken from the red dashed square in (a). (b) PXRD patterns of the obtained senary, septenary, and octonary HEA SNRs. (c) Full discharge−charge curves of HEA-PtPdIrRuAuAg SNRs at 0.10 A g⁻¹. (d) Li-O₂ battery performance of PtPdIrRuAuAg SNRs. Reprinted with permission from ref 99. Copyright 2022, American Chemical Society. (e) Orbital interactions between LiO₂ /Li₂O₂ and catalysts with different d-band centers. (f) The corresponding catalytic effects. Reprinted with permission from ref 100. Copyright 2023, Wiley-VCH.

electron transfer from the alloy surface to the adsorbed species, thereby facilitating electron transfer in the reaction process (Figure 5d). The Ru-4d and Ir-5d electron orbitals were extensively distributed near $E_f$ and overlap with the d orbitals of other metals, enhancing the electron density near $E_f$. Furthermore, it was suggested that the d-band center of HEAs shifting to $E_f$ could improve the electron transfer capability of HEAs.

While HEAs composed of noble metals demonstrate effective catalysis performance in Li-O₂ batteries, their wide application is seriously restricted due to the high cost and scarcity of precious metal bases. It is a strategy for reducing the cost of catalysts to replace some noble metals with other low-priced metals. Tian et al. developed a range of noble and 3d metal HEAs with varying d-band centers using a carbon-thermal shock method.[100] As a catalyst for the Li-O₂ battery cathode, FeCoNiMnPtIr exhibited significantly higher catalytic activity compared with other alloys. Notably, the overpotential of the Li-O₂ battery during recharging was greatly reduced, leading to an improved energy conversion efficiency. The catalytic mechanism of FeCoNiMnPtIr in Li-O₂ batteries could be explained by the Sabatier theory that a moderate d-band center with appropriate adsorption strength propels the higher catalytic activity (Figure 5e). They considered that a high d-band center could excessively interact with oxygen species, hindering the efficient desorption of LiO₂ to Li₂O₂ (Figure 5f). More studies have further optimized the catalytic performance
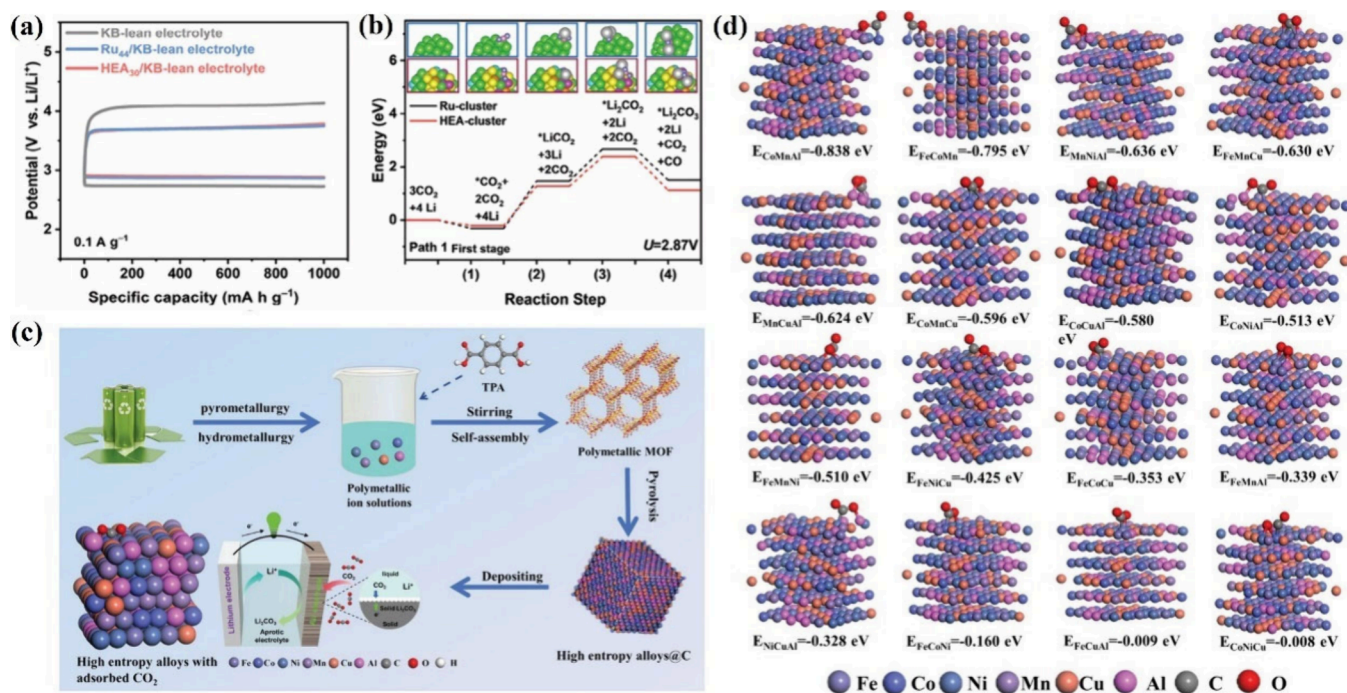
**Figure 6.** (a) Charge and discharge curves for KB, Ru, and NiFeCoCuRu with a lean electrolyte at a current density of 100 mA g$^{-1}$ with a capacity of 1000 mA h g$^{-1}$. (b) Free-energy diagram of Ru-cluster and HEAs-cluster under the equilibrium potentials of Li$^+$|Li$_2$CO$_3$. Reprinted with permission from ref 103. Copyright 2024, Wiley-VCH GmbH. (c) Schematic flow diagram of cycling spent lithium battery as FeCoNiMnCuAl@C for advanced Li-CO$_2$ batteries. (d) Adsorption model ingand adsorption energy at different active sites of FeCoNiMnCuAl@C and CO$_2$, in that order CoMnAl, FeCoMn, MnNiAl, FeMnCu, MnCuAl, CoMnCu, CoCuAl, CoNiAl, FeMnNi, FeNiCu, FeCoCu, FeMnAl, NiCuAl, FeCoNi, FeCuAl, and CoNiCu. Reprinted with permission from ref 104. Copyright 2024, Wiley-VCH GmbH.

of HEAs by designing heterogeneous structures using HEAs with carbons or metals. Wang et al. presented a continuous "droplet-to-particle" approach for producing hollow RuIrFe-CoNi-HEA nanoparticles.[101] This unique alloy structure could enhance catalytic activity and stability, demonstrating 80 cycles for the Li-O$_2$ battery with a capacity cutoff at 4000 mAh g$^{-1}$ at 2000 mA g$^{-1}$. Ru and Ir contributed to high catalytic activity, while Fe, Co, and Ni enhance the stability of the alloy, showcasing the synergistic effect of HEAs. The heterostructure PtRuFeCoNi HEA@Pt was also discussed, revealing that the ORR/OER kinetics could be boosted by electron-rich and electron-deficient sites at the heterointerface of nano-particles.[102] As a result, the Li-O$_2$ battery utilizing HEA@Pt electrocatalyst exhibited the low polarization potential (0.37 V) and the long-term cyclability (210 cycles) under a cutoff capacity of 1000 mAh g$^{-1}$, outperforming many previously reported noble metal-based catalysts.

**4.2. HEAs in Li-CO$_2$ Batteries.** Sun et al. synthesized NiFeCoCuRu with the hexagonal close-packed (HCP) structure on KB, demonstrating the redistribution of electrons and the fine-tuning of electronic structures.[103] The metal–metal distance between Fe, Co, Ni, and Cu atoms was 2.5 Å, while the distance between Ru and other atoms was 2.58 Å, indicating the formation of a solid-solution structure. NiFeCoCuRu as a bifunctional catalyst for the Li-CO$_2$ battery, showed a higher discharge voltage plateau of 2.85 V and a lower recharge potential of 3.6 V (Figure 6a). It also exhibited a higher discharge capacity (>20000 mAh g$^{-1}$) and a long cycle life of 2940 h. Additionally, Li$_2$CO$_3$ could almost completely decompose after recharging. The superior performance of the Li-CO$_2$ battery was attributed to the configurational entropy effect of ultrasmall particles, promoting high activity in electron

transfer on the surface. They demonstrated that there were two fundamental reasons for the excellent performance of the Li-CO$_2$ battery: (1) the d-band center of NiFeCoCuRu was closer to the E$_f$; (2) the surface of the HEA had the active clusters of Ru, Co, and Ni, as well as the active sites of Ru and Cu. The results indicated that HEAs have higher conductivity and lower Gibbs free energy for both the Li$_2$CO$_3$ nucleation and desorption steps compared to those of Ru (Figure 6b).

In addition to the noble metal-based HEAs, non-noble metal HEAs can also be utilized in Li-CO$_2$ batteries. Yi et al. prepared FeCoNiMnCuAl@C with an FCC structure through a one-step carbon thermal reduction process (Figure 6c).[104] The entropy value of FeCoNiMnCuAl was calculated to be 1.79R based on the element content and mixed entropy formula. Numerous lattice distortions and significant internal tensile and compressive stresses were widely observed within the HEAs hierarchical nanosheets, likely stemming from the varying atomic radius and electronegativity of the constituent elements Fe, Co, Ni, Mn, Cu, and Al. Despite slight oxidation of Fe, Co, Ni, Mn, Cu, and Al in FeCoNiMnCuAl@C due to their chemical activities, Li-CO$_2$ batteries utilizing FeCoNi-MnCuAl@C demonstrated a higher discharge plateau (2.77 V), lower overpotential (1.56 V) and superior discharge capability of 27664 mAh g$^{-1}$ at a current density of 100 mA g$^{-1}$. The battery exhibited exceptional durability of 134 cycles and a low overpotential of 1.05 V with a cutoff capacity of 1000 mAh g$^{-1}$ at a constant current density of 100 mA g$^{-1}$. The results indicated that FeCoNiMnCuAl@C displayed favorable bifunctional catalytic activity. The electronic density of states of HEAs was determined using DFT, revealing that HEA possessed typical metal characteristics and good conductivity, resulting in lower electrochemical impedance of the battery.

## Table 1. Performance of Recent HEA Catalysts for Zn-Air Batteries

| Catalyst | Power density/ mW cm$^{-2}$ | Special energy/ Wh kg$_{Zn}$$^{-2}$ | Special capacity/ mAh g$_{Zn}$$^{-1}$ | Open-circuit voltage/V | Benchmarks open-circuit voltage, power density or special energy | Synergy method | Ref |
|---|---|---|---|---|---|---|---|
| FeCoNiMoW | 116.9 | – | 857 | 1.59 | Pt/C and RuO$_2$-based: 1.56 V and 793 mAh g$_{Zn}$$^{-1}$ | Low-temperature oil phase | 108 |
| AlNiCoRuMo | 146 | 851.3 | – | 1.48 | Pt/C-IrO$_2$: 1.42 V, 88.4 mW cm$^{-2}$, 760 Wh kg$_{Zn}$$^{-1}$ | Dealloying | 107 |
| Fe$_6$Ni$_{20}$Co$_2$Mn$_2$Cu$_{1.5}$@rGO | 154 | 800 | – | 1.405 | – | Joule heating strategy | 109 |
| FeNiCoMnRu@CNT | 111 | – | 735 | 1.47 | Pt/C: 1.47 V, 105 mW cm$^{-2}$ | Pyrolysis | 106 |
| AlFeCoNiCr | 125 | 943 | 800 | 1.55 | Pt/C + IrO$_2$-based: 1.41 V, 87 mW cm$^{-2}$ | Dealloying | 115 |
| FeCoNiMnV/N-CNTs | 185 | – | – | 1.482 | Pt/C + RuO$_2$: ~1.440 V, 77.92 mW cm$^{-2}$ | Pyrolysis | 111 |
| Fe$_{12}$Ni$_{23}$Cr$_{10}$Co$_{30}$ Mn$_{25}$/CNT | 128.6 | 865.5 | 760 | 1.38 | Pt/C+RuO$_2$: 1.40 V, 103.3 mW cm$^{-2}$ | Liquid-phase reduction and high temperature sintering | 110 |
| CrMnFeCoNi | 116 | – | 788 | 1.489 | Pt/C-based: 1.204 V, 23.7 mW cm$^{-2}$ | Low-temperature oil phase | 112 |
| FeCoNiMnCu-1000(1:1) | 81 | – | 630.29 | 1.36 | Pt/C-RuO$_2$: 1.38 V | Pyrolysis | 113 |
| CuCoMnNiFe | 16.5 | 481 | 688 | 1.52 | Pt/C−RuO$_2$: 12.2 mW cm$^{-2}$ | Casting-cum-cryomilling method | 114 |
| PtPdAuAgCuIrRu@ (AlNiCoFeCrMoTi)$_3$O$_4$ | 146 | 897.6 | – | 1.528 | Pt/C-IrO$_2$-based: 1.462 V, 103.8 mW cm$^{-2}$, 812.8 Wh kg$^{-1}$ | Alloying−dealloying | 116 |
| Mn$_{70}$Ni$_{7.5}$Cu$_{7.5}$Co$_{4.2}$V$_{4.2}$Fe$_2$Mo$_2$Pd$_{0.5}$Pt$_{0.5}$Au$_{0.5}$Ru$_{0.5}$Ir$_{0.5}$ | 122 | 952 | – | 1.49 | Pt/C-IrO$_2$-based: 1.43 V, 817 Wh kg$_{Zn}$$^{-1}$ | Dealloying | 117 |
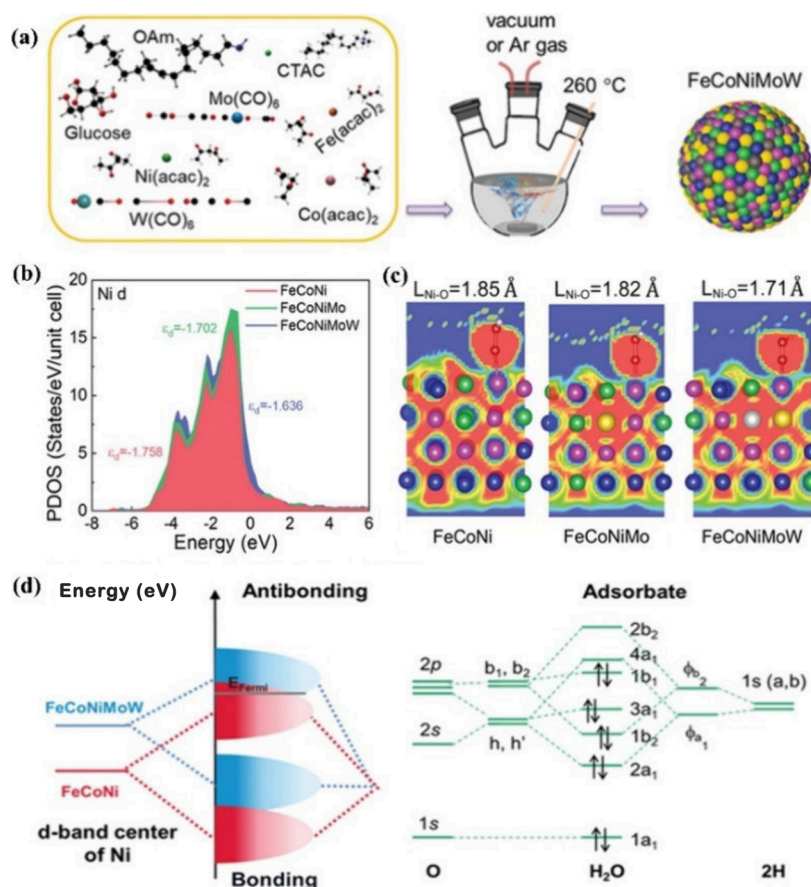


**Figure 7.** (a) Schematic diagram of the colloidal synthesis process used to produce FeCoNiMoW nanoparticles. (b) D-band center position of Ni atoms in alloys by DFT. (c) ELF calculations. (d) Diagram of the hybridization between catalysts of alloys and the O atoms of the H$_2$O molecule. Reprinted with permission from ref 108. Copyright 2017, Wiley-VCH GmbH.
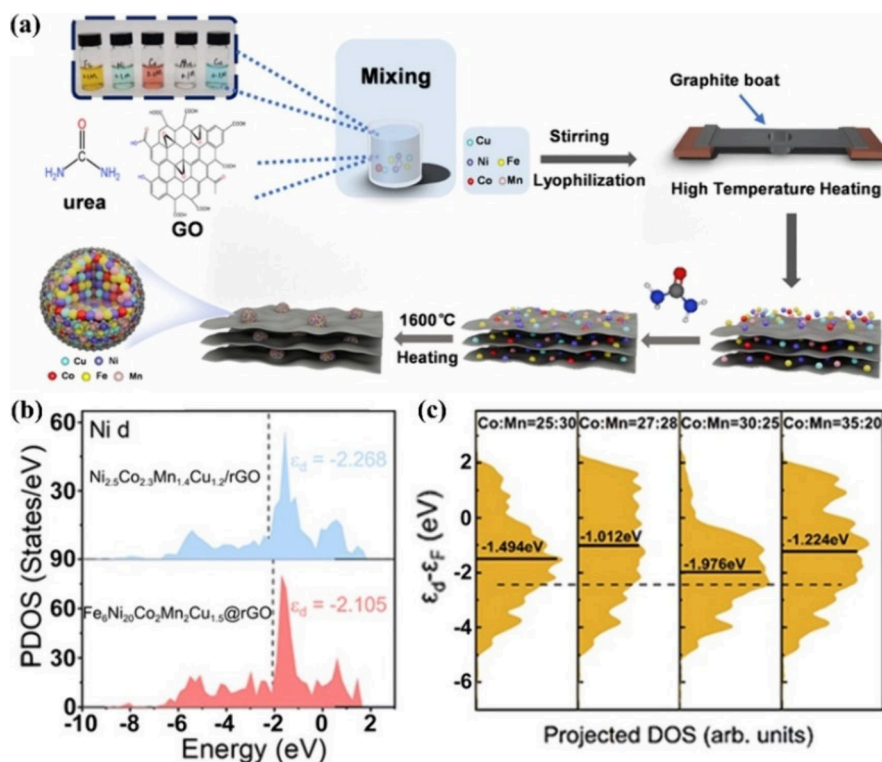
**Figure 8.** (a) Schematic diagram of the preparation of $Fe_6Ni_{20}Co_2Mn_2Cu_{1.5}$@rGO. (b) Projected density of states of Ni 3d orbitals in $Fe_6Ni_{20}Co_2Mn_2Cu_{1.5}$@rGO. Reprinted with permission from ref 109. Copyright 2024, The Royal Society of Chemistry. (c) D-band center of Co in HEAs. Reprinted with permission from ref 110. Copyright 2023, American Chemical Society.

Additionally, the active sites in FeCoNiMnCuAl were simulated. It was demonstrated that the various elements in HEA were able to provide numerous catalytic active sites for electrochemical reactions. However, pinpointing the specific active site of the HEA was challenging due to the random distribution of surface atoms. By examination of 16 potential combinations of surface atoms, it was discovered that each surface exhibited strong $CO_2$ adsorption capacity and activation of inert molecules (Figure 6d). Particularly, the Co, Mn, and Al combination showed the highest adsorption energy.

**4.3. HEAs in Zn-Air Batteries.** HEAs have been extensively studied in the field of water electrolysis.[105] As mentioned above, the reaction mechanism of the Zn-air batteries is similar to the half-reaction of electrolyzing water. Therefore, HEAs are commonly utilized in the catalytic reactions of the ORR/OER in Zn-air batteries. Zhang et al. synthesized a series of HEAs using ultrasonic-assisted wet chemistry.[106] The FeNiCoMnRu@CNT-based Zn-air battery exhibited an open circuit voltage of 1.45 V and a maximum power density of up to 111 mW cm$^{-2}$, which was comparable to that of a Pt/C-based battery (Table 1). The excellent ORR/OER bifunctional catalytic activity could be explained by Ru's ability to alter the electronic structure of the HEA and serve as an active site for the ORR. Jin et al. synthesized Al-based AlNiCoRuMo using a dealloying method. When it was employed in a zinc-air battery, the battery showcased a specific capacity of 851 mAh g$^{-1}$. In this case, Ru and Mo were recognized as crucial elements for enhancing the catalytic activity of alloys.[107] There were also noble-metal-free options for Zn-air batteries. He et al. reported FeCoNiMoW consisting of 3D-metal Fe, Co, Ni, and the electronegativity 4d Mo and 5d W by a colloidal synthesis method (Figure 7a).[108] They

discovered a significant local distortion caused by the superior atom with the d-band center of the Ni site in FeCoNiMoW shifting to $E_f$ (Figure 7b). This greatly enhanced the adsorption of intermediates and led to a faster reaction rate (Figure 7c). Furthermore, compared to other alloys, the d-band center of Ni in FeCoNiMoW was closer to the $E_f$, resulting in a higher antibonding orbital, less electron occupancy in the antibonding orbital, and better bonding orbital (Figure 7d). However, the little dissolution of metals (Mo, Fe, Co, etc.) was also observed after the prolong operation. Gao et al. prepared $Fe_6Ni_{20}Co_2Mn_2Cu_{1.5}$@rGO using a Joule heating method (Figure 8a).[109] Compared to the Fe-free alloys, the d-band center of Ni metal in $Fe_6Ni_{20}Co_2$-$Mn_2Cu_{1.5}$ shifted to the $E_f$, enhancing adsorption abilities and electron transfer rate at the alloy's surface with the reaction intermediate (Figure 8b). Moreover, no structural collapse of the HEA occurred during the cycling process.

Cao et al. synthesized a series of HEAs using liquid-phase reduction and high-temperature sintering methods.[110] They discovered that the Co/Mn ratio impacts the Gibbs free energy between the surface of the HEAs and adsorbed oxygen-containing species. The DFT results revealed that the d-band center of Co in $Fe_{12}Ni_{23}Cr_{10}Co_{30}Mn_{25}$ shifted down the most among these alloys, and the adsorption abilities of the surface Co atoms on $O_2$ was stronger (Figure 8c). The electronic structure of $Fe_{12}Ni_{23}Cr_{10}Co_{30}Mn_{25}$ could accelerate the ORR/OER kinetic processes. When $Fe_{12}Ni_{23}Cr_{10}Co_{30}Mn_{25}$/CNT served as the cathode of the Zn-air batteries, the battery exhibited a specific capacity of 760 mAh g$^{-1}$ and a specific energy of 865.5 Wh kg$^{-1}$. The FeCoNiMnV with multiple adjacent Fe, Co, Ni, Mn, and V promoted random d-band hybridization and displays a continuous and broad binding energy distribution.[111] Thus, it provided sufficient adsorption

sites for oxygen-containing intermediates to accelerate the reaction rate. Meantime, it also exhibited the slow diffusion effect leading to enhancement of the durability of the catalysts. Apart from the elemental composition, lattice distortion significantly affected the physical and chemical properties of the alloys. Severe strains could influence the binding mode and catalytic selectivity of HEA with intermediates. He et al. synthesized a range of ternary, quaternary, and quintary alloys.[112] Among them, the CrMnFeCoNi-based Zn-air battery had an open circuit voltage of 1.489 V and a specific capacity of 836 mAh g$^{-1}$. In comparison to ternary and quaternary alloys, CrMnFeCoNi exhibited a homogeneous structure with numerous defects such as lattice distortions and dislocations. Lattice distortion facilitated a higher density of active electrons near the $E_f$, thereby accelerating the electron transfer rate for ORR/OER. Conversely, CuMnFeCoNi displayed a high density of dislocations in the lattice, along with a CuNi phase, resulting in a lack of homogeneity. Moreover, increasing the twinning of HEAs proved to be an effective method for enhancing the performance of metal catalysts. DFT results indicated a low energy barrier in the ORR/OER of CrMnFeCoNi in the rapid-control step. They considered that the proximity of the d-band center to $E_f$ strengthens the binding between the metal atom and the intermediate. Additionally, the Sabatier principle suggested that the catalyst's catalytic activity peaks with a moderate adsorption energy. Therefore, the d-band center of CrMnFeCoNi fell between the quaternary alloy and CuMnFeCoNi, facilitating the release of $O_2$ during the OER.

Some modified carriers are also used to enhance the catalytic performance of HEAs in Zn-air batteries. FeCoNiMnCu with a particle size of about 100 nm encapsulated in an N-doped hollow carbon tube was designed and manufactured by solid-phase canonization (Figure 9).[113] From Figure 9b, there was very little elemental Zn in the HEA nanoparticles. Zn was melted/evaporated to create a porous structure, increasing the material's specific surface area. When it was utilized in a Zn-air battery, the battery exhibited a specific capacity of 630 mAh g$^{-1}$ and excellent stability. However, some HEAs lost activity when they were run for a long time in Zn-air batteries. The reason was that Zn was discovered on the cathode surface after a long cycle of the battery, affecting the HEAs catalytic effect. Madan et al. found that a small amount of Zn accumulates on the electrode surface after 24 h of operation. This Zn deposition could cover and impact the active sites of the catalyst, resulting in a decrease in the catalytic activity of the HEA.[114]

To clearly demonstrate and compare the catalytic performance and advantages of HEAs in Zn-air batteries, we summarize the recently reported performance of some Zn-air batteries based on HEAs in Table 1, including the reported power density, special energy, special capacity, open-circuit voltage, and comparisons with conventional noble metal-based benchmarks.

From the above research of HEAs in metal-air batteries, it is clear that adjusting the d-band center in HEAs has become one of the hot topics in the catalytic field. Component design can simultaneously meet the requirements for the catalytic activity and stability. The increase of element kinds within HEAs and the size differences among metal atoms lead to significant lattice distortions, which regulate their electronic structures, including the shift of the d-band center, while the cocktail effect demonstrates the synergistic interaction among multiple
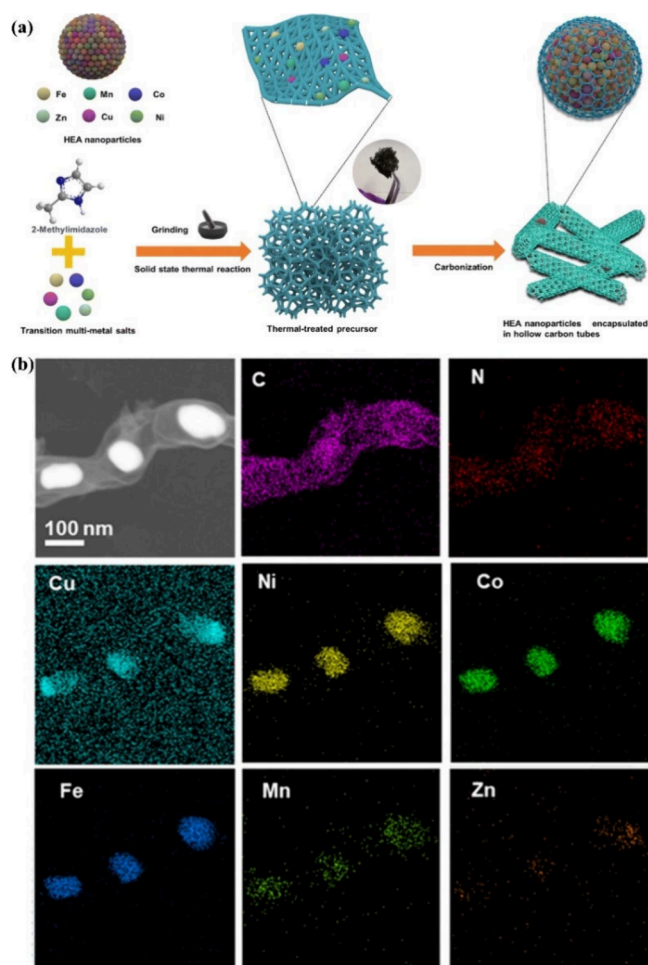


**Figure 9.** (a) Schematic of the synthesis of FeCoNiMnCu nanoparticles encapsulated in N-doped graphitized hollow carbon tubes. (b) EDS mapping of FeCoNiMnCu. Reprinted with permission from ref 113. Copyright 2023, The Royal Society of Chemistry.

elements. The diffusion hysteresis effect enhances the stability of the catalyst to a certain extent. There are three explanations for how the shift in the center of the HEAs d-band affects their catalytic activities, respectively. Some suggests that the d-band center of HEAs shifting to $E_f$ can enhance adsorption strength between the HEAs surface and reactants, thereby increasing the catalytic activity of HEAs.[99,103,108] Another viewpoint argues the opposite, claiming that the downward movement of the d-band center in HEAs is favorable for improving catalytic activity.[102,110] Furthermore, studies have shown that surface Sabatier principles and volcano plots can also explain the relationship between the "d-band center-adsorption strength-the catalytic activity" of HEAs.[100,112] While there is no definitive conclusion regarding these three explanations, many researchers agree that shifting the d-band center of the HEA to $E_f$ can enhance its activity.

## 5. SUMMARY AND PROSPECT

In this review, we first provide a detailed explanation of the reaction mechanisms of Li-O$_2$ batteries, Li-CO$_2$ batteries, and Zn-air batteries as well as their challenges. The issue of sluggish kinetics on the cathode can be promoted by utilizing HEAs to enhance the efficiency of ORR/OER, CO$_2$RR/CO$_2$ER, etc. Subsequently, the synthesis methods and core effects of HEAs

are also reviewed, offering valuable insights into the development and application of these alloys. Then, we summarize recent research on HEAs in metal-air batteries. The main focus is on regulating the electronic structure of the HEAs by adding or substituting certain elements such as shifting the d-band center of the alloys. The adsorption strength of reactants and intermediates on the active sites is influenced by the d-band center of the HEAs, thereby affecting the performance of catalytic reactions and metal-air batteries. Even though HEAs are being extensively studied and applied in metal-air batteries, there are still many issues that require further investigation and explanation. The future developments of HEAs are summarized and prospected in Figure 10.
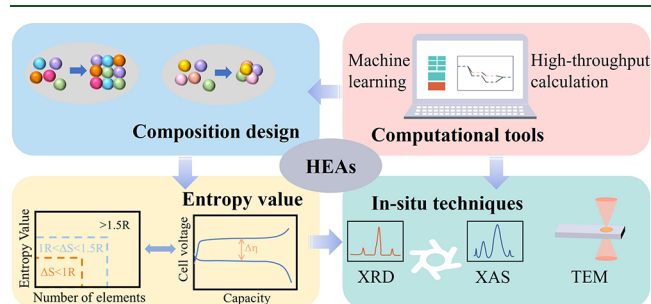


**Figure 10.** Schematic illustration of the future perspectives of HEAs.

1. **Component design and electronic structure control of HEAs.** Although HEAs possess unique structures and properties, the complexity of their composition and structure poses significant challenges to the in-depth research on the application of HEAs. The alloy's performance relies on factors such as its chemical composition and electronic structure. There are still crucial technical challenges to optimize the chemical composition and precisely control the electronic structure. While the rational design of the types and quantities of elements can effectively regulate a material's mechanical properties, corrosion resistance, and thermal stability, the modulation of its electronic structure frequently serves to tailor both its physical attributes, such as electrical and thermal conductivity, and chemical properties, particularly electronegativity, in HEAs. Therefore, by adjusting the components and electronic structure of HEAs, the catalytic properties of ORR/OER or $CO_2RR/CO_2ER$ will be selectively enhanced, effectively addressing the kinetic sluggishness issue in metal-air batteries. Additionally, the stabilities of HEAs in applications such as metal-air batteries are also influenced by their composition.

2. **Machine learning and theoretical computing.** The design space of HEA compositions is vast. Predicting alloy performance solely through traditional trial-and-error methods inevitably leads to the randomness and inaccuracy of research results. Material screening, structure prediction and performance assessment can be carried out quickly and efficiently by utilizing machine learning simulations and high-throughput computing techniques. By establishing suitable machine learning models, researchers can rapidly predict the catalytic performance of HEAs under different elemental compositions, guiding experimental design and material

synthesis. Furthermore, machine learning can assist researchers in optimizing the formulation and process parameters of HEAs, enhancing material performance and design efficiency. High-throughput computing techniques are able to conduct large-scale quantum mechanical simulations and molecular dynamics simulations on computers to explore the microstructures and phase transition processes in HEAs, as well as adsorption energy (reaction activation energy) between HEAs active sites and intermediates within metal-air batteries. Machine learning and theoretical computing can help researchers quickly screen HEAs catalysts for metal-air batteries.

3. **Relationship between entropy value and catalytic activity of HEAs.** HEAs consist of various elements, forming a uniform solid solution with a high-entropy effect. It is well-known that entropy, as a thermodynamic parameter, represents the degree of disorganization of the material structure, and its value can reflect the material structural stability to a certain extent. The entropy value of HEAs shows a significant correlation with the complex arrangement of atoms in the alloy's structure. At the same time, the electronic configuration of atoms on the surface of the alloy is closely linked to its catalytic performance. Yet, the exact connections between the entropy value of HEA catalysts and their catalytic activities are still unclear. Investigating the intrinsic connections between entropy values, microstructure, and catalytic performance can provide theoretical support for the development of HEAs in metal air batteries.

4. **The catalytic mechanism study by in-situ technologies.** The catalytic activity of catalysts is primarily achieved through surface adsorption and electron transfer steps. So far, the mechanism of HEAs with high catalytic activity in metal-air batteries is still unclear. For example, how the d-band centers of HEAs shift or how the adsorption energy between the HEAs and reactants/intermediates changes are conducive to catalytic reactions. In other words, it is not yet clear how the electronic structure of HEAs can be controlled to regulate the ORR/OER and $CO_2RR/CO_2ER$ for metal-air batteries. The advancement of in situ surface technology can enhance our understanding of the role of metal atoms in HEAs in catalytic reactions and how to adjust the catalytic activity in metal-air batteries. For instance, in situ X-ray diffraction (XRD) is able to observe the formation and decomposition of products during the reaction. In-situ transmission electron microscopy (TEM) and scanning electron microscopy (SEM) techniques are able to observe the growth, morphology, and composition changes of reaction intermediates or final products on the surface of HEA catalysts in real-time. In-situ X-ray photoelectron spectroscopy (XPS) and X-ray absorption spectroscopy (XAS) can offer insights into whether the chemical valence states and electronic structures of elements in HEAs alter during electrochemical reactions. By utilizing in situ techniques to track structural changes and pinpoint the active sites in the electrochemical process, researchers can acquire valuable insights into the structure-performance relationship of HEAs. Hence, the development of diverse in situ technologies is crucial

for a comprehensive understanding of HEAs for metal-air batteries and other catalytic energy storage systems. Moreover, the high cost of HEA raw materials poses a challenge to large-scale production, and finding ways to reduce costs remains a significant issue in HEAs research.

## AUTHOR INFORMATION

**Corresponding Authors**

**Xiaowei Mu** — *School of Materials Science and Engineering, Herbert Gleiter Institute of Nanoscience, Nanjing University of Science and Technology, Nanjing, Jiangsu 210094, China;* ⓞ orcid.org/0000-0001-5276-7754; Email: xiaoweimu@njust.edu.cn

**Zhu Cheng** — *Section Storage of Electrochemical Energy, Radiation Science and Technology, Faculty of Applied Sciences, Delft University of Technology, 2629 JB Delft, The Netherlands;* ⓞ orcid.org/0000-0002-9997-0781; Email: z.cheng@tudelft.nl

**Authors**

**Xueping Zhang** — *School of Materials Science and Engineering, Jiangsu University, Zhenjiang 212013, China*

**Yunjian Liu** — *School of Materials Science and Engineering, Jiangsu University, Zhenjiang 212013, China;* ⓞ orcid.org/0000-0002-8729-1351

**Xiaohua Zhao** — *School of Materials Science and Engineering, Jiangsu University, Zhenjiang 212013, China*

Complete contact information is available at:
https://pubs.acs.org/10.1021/acs.energyfuels.4c03386

**Notes**

The authors declare no competing financial interest.

**Biographies**

Xueping Zhang received her Ph.D. degree at Nanjing University in 2020, under the supervision of Prof. Haoshen Zhou and Prof. Ping He. She currently serves as a laboratory technician at Jiangsu University. Her research interests mainly focus on catalysts design and mechanism exploration in Li-air batteries.

Yunjian Liu obtained his Ph.D. degree in 2009 from Central South University. He worked as a postdoctoral at Chery Automobile Co. Ltd. from 2011 to 2013 and a visiting scholar at Lawrence Berkeley National Laboratory from 2015 to 2016. He is currently a professor in the School of Material Science and Engineering at Jiangsu University. His research interest focuses on advanced energy materials for lithium/sodium ion batteries and various energy storage systems.

Xiaohua Zhao received her Ph.D. degree in materials science and engineering from Shandong University in 2011, under the supervision of Prof. Guanghui Min. She currently serves as a senior experimentalist at Jiangsu University. Her research interests include energy conversion and storage, and photocatalytic hydrogen evolution.

Zhu Cheng received his B.S. degree in Nanjing University in 2016, and received his Ph.D. degree in Nanjing University in 2021 under the supervision of Prof. Haoshen Zhou and Prof. Ping He. He currently is working in Delft University of Technology as a postdoctoral researcher. His research interests mainly focus on the synthesis and application of halide solid electrolytes in all-solid-state Li batteries.

Xiaowei Mu received her B.S. degree at Nanjing University of Aeronautics and Astronautics in 2015 and her Ph.D. degree at Nanjing University in 2020, under the supervision of Prof. Haoshen

Zhou and Prof. Ping He. She currently is an associate professor of School of Materials Science and Engineering at Nanjing University of Science and Technology. Her research interests mainly focus on electrochemical functional materials design and mechanism exploration in Li-air batteries.

## ACKNOWLEDGMENTS

## REFERENCES

(1) Schmidt, O.; Hawkes, A.; Gambhir, A.; Staffell, I. The future cost of electrical energy storage based on experience rates. *Nature Energy* **2017**, *2* (8), 17110.

(2) Sharma, R.; Kumar, H.; Kumar, G.; Sharma, S.; Aneja, R.; Sharma, A. K.; Kumar, R.; Kumar, P. Progress and challenges in electrochemical energy storage devices: Fabrication, electrode material, and economic aspects. *Chemical Engineering Journal* **2023**, *468*, 143706.

(3) Tang, L.; Peng, H.; Kang, J.; Chen, H.; Zhang, M.; Liu, Y.; Kim, D. H.; Liu, Y.; Lin, Z. Zn-based batteries for sustainable energy storage: strategies and mechanisms. *Chem. Soc. Rev.* **2024**, *53* (10), 4877−4925.

(4) Gourley, S. W. D.; Brown, R.; Adams, B. D.; Higgins, D. Zinc-ion batteries for stationary energy storage. *Joule* **2023**, *7* (7), 1415−1436.

(5) Wen, B.; Huang, Y.; Jiang, Z.; Wang, Y.; Hua, W.; Indris, S.; Li, F. Exciton Dissociation into Charge Carriers in Porphyrinic Metal-Organic Frameworks for Light-Assisted Li-O$_2$ Batteries. *Adv. Mater.* **2024**, *36* (32), 2405440.

(6) Freunberger, S. A.; Chen, Y.; Peng, Z.; Griffin, J. M.; Hardwick, L. J.; Bardé, F.; Novák, P.; Bruce, P. G. Reactions in the Rechargeable Lithium-O$_2$ Battery with Alkyl Carbonate Electrolytes. *J. Am. Chem. Soc.* **2011**, *133* (20), 8040−8047.

(7) Harding, J. R.; Amanchukwu, C. V.; Hammond, P. T.; Shao-Horn, Y. Instability of Poly(ethylene oxide) upon Oxidation in Lithium-Air Batteries. *J. Phys. Chem. C* **2015**, *119* (13), 6947−6955.

(8) Li, Y.; Wang, X.; Dong, S.; Chen, X.; Cui, G. Recent Advances in Non-Aqueous Electrolyte for Rechargeable Li-O$_2$ Batteries. *Adv. Energy Mater.* **2016**, *6* (18), 1600751.

(9) Qiu, D.; Li, B.; Zhao, C.; Dang, J.; Chen, G.; Qiu, H.; Miao, H. A review on zinc electrodes in alkaline electrolyte: Current challenges and optimization strategies. *Energy Storage Materials* **2023**, *61*, 102903.

(10) Huang, Y.; Wang, Y.; Tang, C.; Wang, J.; Zhang, Q.; Wang, Y.; Zhang, J. Atomic Modulation and Structure Design of Carbons for Bifunctional Electrocatalysis in Metal-Air Batteries. *Adv. Mater.* **2019**, *31* (13), 1803800.

(11) Huang, Z.-F.; Wang, J.; Peng, Y.; Jung, C.-Y.; Fisher, A.; Wang, X. Design of Efficient Bifunctional Oxygen Reduction/Evolution Electrocatalyst: Recent Advances and Perspectives. *Adv. Energy Mater.* **2017**, *7* (23), 1700544.

(12) Wang, Z.-L.; Xu, D.; Xu, J.-J.; Zhang, X.-B. Oxygen electrocatalysts in metal-air batteries: from aqueous to nonaqueous electrolytes. *Chem. Soc. Rev.* **2014**, *43* (22), 7746−7786.

(13) Sun, Q.; Li, X.-H.; Wang, K.-X.; Ye, T.-N.; Chen, J.-S. Inorganic non-carbon supported Pt catalysts and synergetic effects for oxygen reduction reaction. *Energy Environ. Sci.* **2023**, *16* (5), 1838−1869.

(14) Zhu, Z.; Lv, Q.; Ni, Y.; Gao, S.; Geng, J.; Liang, J.; Li, F. Internal Electric Field and Interfacial Bonding Engineered Step-Scheme Junction for a Visible-Light-Involved Lithium-Oxygen Battery. *Angew. Chem., Int. Ed.* **2022**, *61* (12), No. e202116699.

(15) Jiang, Z.; Wen, B.; Huang, Y.; Guo, Y.; Wang, Y.; Li, F. New Reaction Pathway of Superoxide Disproportionation Induced by a

Soluble Catalyst in Li-O$_2$ Batteries. *Angew. Chem., Int. Ed.* **2024**, *63* (1), No. e202315314.

(16) Lv, Q.; Zhu, Z.; Ni, Y.; Wen, B.; Jiang, Z.; Fang, H.; Li, F. Atomic Ruthenium-Riveted Metal-Organic Framework with Tunable d-Band Modulates Oxygen Redox for Lithium-Oxygen Batteries. *J. Am. Chem. Soc.* **2022**, *144* (50), 23239−23246.

(17) Zhang, X.; Zhang, Q.; Wang, X.-G.; Wang, C.; Chen, Y.-N.; Xie, Z.; Zhou, Z. An Extremely Simple Method for Protecting Lithium Anodes in Li-O$_2$ Batteries. *Angew. Chem., Int. Ed.* **2018**, *57* (39), 12814−12818.

(18) Yu, Y.; Huang, G.; Wang, J.-Z.; Li, K.; Ma, J.-L.; Zhang, X.-B. In Situ Designing a Gradient Li$^+$ Capture and Quasi-Spontaneous Diffusion Anode Protection Layer toward Long-Life Li-O$_2$ Batteries. *Adv. Mater.* **2020**, *32* (38), 2004157.

(19) Bi, X.; Jiang, Y.; Chen, R.; Du, Y.; Zheng, Y.; Yang, R.; Wang, R.; Wang, J.; Wang, X.; Chen, Z. Rechargeable Zinc-Air versus Lithium-Air Battery: from Fundamental Promises Toward Technological Potentials. *Adv. Energy Mater.* **2024**, *14* (6), 2302388.

(20) Wang, Q.; Ren, L.; Lu, T.; Wang, S.; Jiang, Z.; Chandio, I. A.; Guan, L.; Hou, L.; Du, H.; Wei, H.; et al. Air-Stable Lithium Metal Anodes: A Perspective of Surface Engineering from Different Dimensions. *ACS Energy Letters* **2023**, *8* (10), 4441−4464.

(21) Wang, L.; Snihirova, D.; Deng, M.; Vaghefinazari, B.; Xu, W.; Höche, D.; Lamaka, S. V.; Zheludkevich, M. L. Sustainable aqueous metal-air batteries: An insight into electrolyte system. *Energy Storage Materials* **2022**, *52*, 573−597.

(22) Xie, W.; Zhu, K.; Yang, H.; Yang, W. Advancements in Achieving High Reversibility of Zinc Anode for Alkaline Zinc-Based Batteries. *Adv. Mater.* **2023**, *36* (5), 2306154.

(23) Al Zoubi, W.; Putri, R. A. K.; Abukhadra, M. R.; Ko, Y. G. Recent experimental and theoretical advances in the design and science of high-entropy alloy nanoparticles. *Nano Energy* **2023**, *110*, 108362.

(24) Yao, Y.; Dong, Q.; Brozena, A.; Luo, J.; Miao, J.; Chi, M.; Wang, C.; Kevrekidis, I. G.; Ren, Z. J.; Greeley, J.; et al. High-entropy nanoparticles: Synthesis-structure-property relationships and data-driven discovery. *Science* **2022**, *376* (6589), No. eabn3103.

(25) Liu, D.; Guo, P.; Pan, H.; Wu, R. Emerging high-entropy compounds for electrochemical energy storage and conversion. *Prog. Mater. Sci.* **2024**, *145*, 101300.

(26) Chen, S.; Wang, Y.; Pu, G.; Xue, Y.; Zhang, K.; Huang, Y. High-Entropy Materials: Controllable Synthesis, Deep Characterization, Electrochemical Energy Application, and Outlook. *Energy Fuels* **2023**, *37* (1), 36−57.

(27) Zhang, R.; Zhang, Y.-C.; Pan, L.; Shen, G.-Q.; Mahmood, N.; Ma, Y.-H.; Shi, Y.; Jia, W.; Wang, L.; Zhang, X.; et al. Engineering Cobalt Defects in Cobalt Oxide for Highly Efficient Electrocatalytic Oxygen Evolution. *ACS Catal.* **2018**, *8* (5), 3803−3811.

(28) Chen, Y.; Zheng, X.; Yang, Y.; Wang, P.; Sun, W. Palladium Metallene-Based Electrocatalysts for Energy Conversion Applications. *Adv. Funct. Mater.* **2024**, 2404408.

(29) Liu, S.; Miao, W.; Ma, K.; Teng, H.; Zhang, X.; Li, J.; Li, W.; Cui, X.; Jiang, L. Defect-rich AuCu@Ag nanowires with exclusive strain effect accelerate nitrate reduction to ammonia. *Applied Catalysis B: Environment and Energy* **2024**, *350*, 123919.

(30) Lei, Y.; Zhang, L.; Xu, W.; Xiong, C.; Chen, W.; Xiang, X.; Zhang, B.; Shang, H. Carbon-supported high-entropy Co-Zn-Cd-Cu-Mn sulfide nanoarrays promise high-performance overall water splitting. *Nano Research* **2022**, *15* (7), 6054−6061.

(31) Zhou, J.; Cheng, J.; Wang, B.; Peng, H.; Lu, J. Flexible metal-gas batteries: a potential option for next-generation power accessories for wearable electronics. *Energy Environ. Sci.* **2020**, *13* (7), 1933−1970.

(32) Kwak, W.-J.; Rosy; Sharon, D.; Xia, C.; Kim, H.; Johnson, L. R.; Bruce, P. G.; Nazar, L. F.; Sun, Y.-K.; Frimer, A. A.; et al. Lithium-Oxygen Batteries and Related Systems: Potential, Status, and Future. *Chem. Rev.* **2020**, *120* (14), 6626−6683.

(33) Sarkar, A.; Dharmaraj, V. R.; Yi, C.-H.; Iputera, K.; Huang, S.-Y.; Chung, R.-J.; Hu, S.-F.; Liu, R.-S. Recent Advances in

Rechargeable Metal-CO$_2$ Batteries with Nonaqueous Electrolytes. *Chem. Rev.* **2023**, *123* (15), 9497−9564.

(34) Du, D.; Zhu, Z.; Chan, K.-Y.; Li, F.; Chen, J. Photo-electrochemistry of oxygen in rechargeable Li-O$_2$ batteries. *Chem. Soc. Rev.* **2022**, *51* (6), 1846−1860.

(35) Cho, S.; Jung, H.; Park, M.; Lyu, L.; Kang, Y.-M. Modulating the Configuration of Air Cathodes toward the Extended Triple-Phase Boundaries of Li-O$_2$ Batteries. *ACS Energy Letters* **2024**, *9* (6), 2848−2857.

(36) Lyu, Z.; Zhou, Y.; Dai, W.; Cui, X.; Lai, M.; Wang, L.; Huo, F.; Huang, W.; Hu, Z.; Chen, W. Recent advances in understanding of the mechanism and control of Li$_2$O$_2$ formation in aprotic Li-O$_2$ batteries. *Chem. Soc. Rev.* **2017**, *46* (19), 6046−6072.

(37) Huang, J.; Peng, Z. Understanding the Reaction Interface in Lithium-Oxygen Batteries. *Batteries & Supercaps* **2019**, *2* (1), 37−48.

(38) Dong, S.; Yang, S.; Chen, Y.; Kuss, C.; Cui, G.; Johnson, L. R.; Gao, X.; Bruce, P. G. Singlet oxygen and dioxygen bond cleavage in the aprotic lithium-oxygen battery. *Joule* **2022**, *6* (1), 185−192.

(39) Radin, M. D.; Rodriguez, J. F.; Tian, F.; Siegel, D. J. Lithium Peroxide Surfaces Are Metallic, While Lithium Oxide Surfaces Are Not. *J. Am. Chem. Soc.* **2012**, *134* (2), 1093−1103.

(40) Varley, J. B.; Viswanathan, V.; Nørskov, J. K.; Luntz, A. C. Lithium and oxygen vacancies and their role in Li$_2$O$_2$ charge transport in Li-O$_2$ batteries. *Energy Environ. Sci.* **2014**, *7* (2), 720−727.

(41) Yang, S.; Qiao, Y.; He, P.; Liu, Y.; Cheng, Z.; Zhu, J.-j.; Zhou, H. A reversible lithium-CO$_2$ battery with Ru nanoparticles as a cathode catalyst. *Energy Environ. Sci.* **2017**, *10* (4), 972−978.

(42) Mu, X.; He, P.; Zhou, H. Toward Practical Li-CO$_2$ Batteries: Mechanisms, Catalysts, and Perspectives. *Accounts of Materials Research* **2024**, *5* (4), 467−478.

(43) Feng, N.; Wang, B.; Yu, Z.; Gu, Y.; Xu, L.; Ma, J.; Wang, Y.; Xia, Y. Mechanism-of-Action Elucidation of Reversible Li-CO$_2$ Batteries Using the Water-in-Salt Electrolyte. *ACS Appl. Mater. Interfaces* **2021**, *13* (6), 7396−7404.

(44) Hou, Y.; Wang, J.; Liu, L.; Liu, Y.; Chou, S.; Shi, D.; Liu, H.; Wu, Y.; Zhang, W.; Chen, J. Mo$_2$C/CNT: An Efficient Catalyst for Rechargeable Li-CO$_2$ Batteries. *Adv. Funct. Mater.* **2017**, *27* (27), 1700564.

(45) Qi, G.; Zhang, J.; Cheng, J.; Wang, B. Freestanding Mo$_3$N$_2$ nanotubes for long-term stabilized 2e$^-$ intermediate-based high energy efficiency Li-CO$_2$ batteries. *SusMat* **2023**, *3* (2), 276−288.

(46) Zhang, Z.; Bai, W.-L.; Cai, Z.-P.; Cheng, J.-H.; Kuang, H.-Y.; Dong, B.-X.; Wang, Y.-B.; Wang, K.-X.; Chen, J.-S. Enhanced Electrochemical Performance of Aprotic Li-CO$_2$ Batteries with a Ruthenium-Complex-Based Mobile Catalyst. *Angew. Chem., Int. Ed.* **2021**, *60* (30), 16404−16408.

(47) Sun, X.; Mu, X.; Zheng, W.; Wang, L.; Yang, S.; Sheng, C.; Pan, H.; Li, W.; Li, C.-H.; He, P.; et al. Binuclear Cu complex catalysis enabling Li-CO$_2$ battery with a high discharge voltage above 3.0 V. *Nat. Commun.* **2023**, *14* (1), 536.

(48) Mahne, N.; Renfrew, S. E.; McCloskey, B. D.; Freunberger, S. A. Electrochemical Oxidation of Lithium Carbonate Generates Singlet Oxygen. *Angew. Chem., Int. Ed.* **2018**, *57* (19), 5529−5533.

(49) Cao, D.; Tan, C.; Chen, Y. Oxidative decomposition mechanisms of lithium carbonate on carbon substrates in lithium battery chemistries. *Nat. Commun.* **2022**, *13* (1), 4908.

(50) Yang, S.; He, P.; Zhou, H. Exploring the electrochemical reaction mechanism of carbonate oxidation in Li-air/CO$_2$ battery through tracing missing oxygen. *Energy Environ. Sci.* **2016**, *9* (5), 1650−1654.

(51) Qiao, Y.; Yi, J.; Wu, S.; Liu, Y.; Yang, S.; He, P.; Zhou, H. Li-CO$_2$ Electrochemistry: A New Strategy for CO$_2$ Fixation and Energy Storage. *Joule* **2017**, *1* (2), 359−370.

(52) Zhang, F.; Zhang, W.; Yuwono, J. A.; Wexler, D.; Fan, Y.; Zou, J.; Liang, G.; Sun, L.; Guo, Z. Catalytic role of in-situ formed C-N species for enhanced Li$_2$CO$_3$ decomposition. *Nat. Commun.* **2024**, *15* (1), 3393.

(53) Li, Y.; Gong, M.; Liang, Y.; Feng, J.; Kim, J.-E.; Wang, H.; Hong, G.; Zhang, B.; Dai, H. Advanced zinc-air batteries based on

high-performance hybrid electrocatalysts. *Nat. Commun.* **2013**, *4* (1), 1805.

(54) Zhao, Z.; Fan, X.; Ding, J.; Hu, W.; Zhong, C.; Lu, J. Challenges in Zinc Electrodes for Alkaline Zinc-Air Batteries: Obstacles to Commercialization. *ACS Energy Letters* **2019**, *4* (9), 2259−2270.

(55) Wang, Q.; Kaushik, S.; Xiao, X.; Xu, Q. Sustainable zinc-air battery chemistry: advances, challenges and prospects. *Chem. Soc. Rev.* **2023**, *52* (17), 6139−6190.

(56) Han, Y.; Zhao, Y.; Yu, Y. Research progress of Zn-air batteries suitable for extreme temperatures. *Energy Storage Materials* **2024**, *69*, 103429.

(57) Rahman, M. A.; Wang, X.; Wen, C. High Energy Density Metal-Air Batteries: A Review. *J. Electrochem. Soc.* **2013**, *160* (10), A1759.

(58) Wu, Y.; Zhang, Y.; Ma, Y.; Howe, J. D.; Yang, H.; Chen, P.; Aluri, S.; Liu, N. Ion-Sieving Carbon Nanoshells for Deeply Rechargeable Zn-Based Aqueous Batteries. *Adv. Energy Mater.* **2018**, *8* (36), 1802470.

(59) Pan, J.; Xu, Y. Y.; Yang, H.; Dong, Z.; Liu, H.; Xia, B. Y. Advanced Architectures and Relatives of Air Electrodes in Zn-Air Batteries. *Advanced Science* **2018**, *5* (4), 1700691.

(60) Jiang, Z.; Huang, Y.; Zhu, Z.; Gao, S.; Lv, Q.; Li, F. Quenching singlet oxygen via intersystem crossing for a stable Li-$O_2$ battery. *Proc. Natl. Acad. Sci. U. S. A.* **2022**, *119* (34), No. e2202835119.

(61) McCloskey, B. D.; Speidel, A.; Scheffler, R.; Miller, D. C.; Viswanathan, V.; Hummelshøj, J. S.; Nørskov, J. K.; Luntz, A. C. Twin Problems of Interfacial Carbonate Formation in Nonaqueous Li-$O_2$ Batteries. *J. Phys. Chem. Lett.* **2012**, *3* (8), 997−1001.

(62) Tong, Z.; Lv, C.; Zhou, Y.; Yin, Z.-W.; Wu, Z.-P.; Li, J.-T. An integrally bilayered flexible cathode woven from CNTs for homogeneous hosting and fast electrocatalytic conversion of $Li_2O_2$ in Li-$O_2$ battery. *Energy Storage Materials* **2024**, *67*, 103301.

(63) Mu, X.; Xia, C.; Gao, B.; Guo, S.; Zhang, X.; He, J.; Wang, Y.; Dong, H.; He, P.; Zhou, H. Two-dimensional Mo-based compounds for the Li-$O_2$ batteries: Catalytic performance and electronic structure studies. *Energy Storage Materials* **2021**, *41*, 650−655.

(64) Zhou, Y.; Gu, Q.; Yin, K.; Li, Y.; Tao, L.; Tan, H.; Yang, Y.; Guo, S. Engineering eg Orbital Occupancy of Pt with Au Alloying Enables Reversible Li-$O_2$ Batteries. *Angew. Chem., Int. Ed.* **2022**, *61* (26), No. e202201416.

(65) Xiao, Y.; Hu, S.; Miao, Y.; Gong, F.; Chen, J.; Wu, M.; Liu, W.; Chen, S. Recent Progress in Hot Spot Regulated Strategies for Catalysts Applied in Li-$CO_2$ Batteries. *Small* **2024**, *20* (1), 2305009.

(66) Hu, C.; Dai, Q.; Dai, L. Multifunctional carbon-based metal-free catalysts for advanced energy conversion and storage. *Cell Reports Physical Science* **2021**, *2* (2), 100328.

(67) Zhang, Z.; Bai, W.-L.; Wang, K.-X.; Chen, J.-S. Electrocatalyst design for aprotic Li-$CO_2$ batteries. *Energy Environ. Sci.* **2020**, *13* (12), 4717−4737.

(68) Yeh, J.-W. Alloy Design Strategies and Future Trends in High-Entropy Alloys. *JOM* **2013**, *65* (12), 1759−1771.

(69) Yi, L.; Xiao, S.; Wei, Y.; Li, D.; Wang, R.; Guo, S.; Hu, W. Free-standing high-entropy alloy plate for efficient water oxidation catalysis: structure/composition evolution and implication of high-valence metals. *Chemical Engineering Journal* **2023**, *469*, 144015.

(70) Suhadolnik, L.; Bele, M.; Smiljanić, M.; Dražić, G.; Rafailović, L. D.; Neumüller, D.; Šala, M.; Logar, A.; Hodnik, N.; Gaberšček, M.; et al. Enhancing oxygen evolution functionality through anodization and nitridation of compositionally complex alloy. *Materials Today Chemistry* **2024**, *35*, 101835.

(71) Liu, H.; Qin, H.; Kang, J.; Ma, L.; Chen, G.; Huang, Q.; Zhang, Z.; Liu, E.; Lu, H.; Li, J.; et al. A freestanding nanoporous NiCoFeMoMn high-entropy alloy as an efficient electrocatalyst for rapid water splitting. *Chemical Engineering Journal* **2022**, *435*, 134898.

(72) Cai, Z.-X.; Goou, H.; Ito, Y.; Tokunaga, T.; Miyauchi, M.; Abe, H.; Fujita, T. Nanoporous ultra-high-entropy alloys containing fourteen elements for water splitting electrocatalysis. *Chemical Science* **2021**, *12* (34), 11306−11315.

(73) Jin, Z.; Lyu, J.; Zhao, Y.-L.; Li, H.; Chen, Z.; Lin, X.; Xie, G.; Liu, X.; Kai, J.-J.; Qiu, H.-J. Top-Down Synthesis of Noble Metal Particles on High-Entropy Oxide Supports for Electrocatalysis. *Chem. Mater.* **2021**, *33* (5), 1771−1780.

(74) Strozi, R. B.; Leiva, D. R.; Huot, J.; Botta, W. J.; Zepon, G. Synthesis and hydrogen storage behavior of Mg-V-Al-Cr-Ni high entropy alloys. *Int. J. Hydrogen Energy* **2021**, *46* (2), 2351−2361.

(75) Yang, P.; Shi, Y.; Xia, T.; Jiang, Z.; Ren, X.; Liang, L.; Shao, Q.; Zhu, K. Novel self-supporting thin film electrodes of FeCoNiCrMn high entropy alloy for excellent oxygen evolution reaction. *J. Alloys Compd.* **2023**, *938*, 168582.

(76) Wang, S.; Xu, B.; Huo, W.; Feng, H.; Zhou, X.; Fang, F.; Xie, Z.; Shang, J. K.; Jiang, J. Efficient FeCoNiCuPd thin-film electro-catalyst for alkaline oxygen and hydrogen evolution reactions. *Applied Catalysis B: Environmental* **2022**, *313*, 121472.

(77) Huang, C.-L.; Lin, Y.-G.; Chiang, C.-L.; Peng, C.-K.; Senthil Raja, D.; Hsieh, C.-T.; Chen, Y.-A.; Chang, S.-Q.; Yeh, Y.-X.; Lu, S.-Y. Atomic scale synergistic interactions lead to breakthrough catalysts for electrocatalytic water splitting. *Applied Catalysis B: Environmental* **2023**, *320*, 122016.

(78) Yu, H.; Chen, W.; Liu, Z.; Du, C. Self-supported amorphous high entropy alloy/crystalline $Ni_2P$ heterostructure for water oxidation under alkaline condition. *Colloids Surf., A* **2024**, *686*, 133354.

(79) Bertelsen, A. D.; Hansen, A. R.; Broge, N. L. N.; Mamakhel, A.; Bondesgaard, M.; Iversen, B. B. Composition space of PtIrPdRhRu high entropy alloy nanoparticles synthesized by solvothermal reactions. *Chem. Commun.* **2022**, *58* (91), 12672−12675.

(80) Zhan, C.; Xu, Y.; Bu, L.; Zhu, H.; Feng, Y.; Yang, T.; Zhang, Y.; Yang, Z.; Huang, B.; Shao, Q.; et al. Subnanometer high-entropy alloy nanowires enable remarkable hydrogen oxidation catalysis. *Nat. Commun.* **2021**, *12* (1), 6261.

(81) Kang, Y.; Cretu, O.; Kikkawa, J.; Kimoto, K.; Nara, H.; Nugraha, A. S.; Kawamoto, H.; Eguchi, M.; Liao, T.; Sun, Z.; et al. Mesoporous multimetallic nanospheres with exposed highly entropic alloy sites. *Nat. Commun.* **2023**, *14* (1), 4182.

(82) Sun, Y.; Zhang, W.; Zhang, Q.; Li, Y.; Gu, L.; Guo, S. A general approach to high-entropy metallic nanowire electrocatalysts. *Matter* **2023**, *6* (1), 193−205.

(83) Zhang, H.-M.; Zhang, S.-F.; Zuo, L.-H.; Li, J.-K.; Guo, J.-X.; Wang, P.; Sun, J.-F.; Dai, L. Recent advances of high-entropy electrocatalysts for water electrolysis by electrodeposition technology: a short review. *Rare Metals* **2024**, *43* (6), 2371−2390.

(84) Bian, H.; Wang, R.; Zhang, K.; Zheng, H.; Wen, M.; Li, Z.; Li, Z.; Wang, G.; Xie, G.; Liu, X.; et al. Facile electrodeposition synthesis and super performance of nano-porous Ni-Fe-Cu-Co-W high entropy alloy electrocatalyst. *Surf. Coat. Technol.* **2023**, *459*, 129407.

(85) Chang, S.-Q.; Cheng, C.-C.; Cheng, P.-Y.; Huang, C.-L.; Lu, S.-Y. Pulse electrodeposited FeCoNiMnW high entropy alloys as efficient and stable bifunctional electrocatalysts for acidic water splitting. *Chemical Engineering Journal* **2022**, *446*, 137452.

(86) Raj, G.; Nandan, R.; Kumar, K.; Gorle, D. B.; Mallya, A. B.; Osman, S. M.; Na, J.; Yamauchi, Y.; Nanda, K. K. High entropy alloying strategy for accomplishing quintuple-nanoparticles grafted carbon towards exceptional high-performance overall seawater splitting. *Materials Horizons* **2023**, *10* (11), 5032−5044.

(87) Gao, S.; Hao, S.; Huang, Z.; Yuan, Y.; Han, S.; Lei, L.; Zhang, X.; Shahbazian-Yassar, R.; Lu, J. Synthesis of high-entropy alloy nanoparticles on supports by the fast moving bed pyrolysis. *Nat. Commun.* **2020**, *11* (1), 2016.

(88) Zhao, J.; Wang, Z.; Fang, X.; Yang, L.; Wu, C.; Gan, W.; Zhou, Y.; Shan, L.; Lin, Y. Fast joule heating synthesis of NiCoFeCrMo high-entropy alloy embedded in graphene for water oxidation. *J. Alloys Compd.* **2023**, *966*, 171535.

(89) Tang, J.; Xu, J. L.; Ye, Z. G.; Li, X. B.; Luo, J. M. Microwave sintered porous CoCrFeNiMo high entropy alloy as an efficient electrocatalyst for alkaline oxygen evolution reaction. *Journal of Materials Science & Technology* **2021**, *79*, 171−177.

(90) Maulana, A. L.; Chen, P.-C.; Shi, Z.; Yang, Y.; Lizandara-Pueyo, C.; Seeler, F.; Abruña, H. D.; Muller, D.; Schierle-Arndt, K.; Yang, P. Understanding the Structural Evolution of IrFeCoNiCu High-Entropy Alloy Nanoparticles under the Acidic Oxygen Evolution Reaction. *Nano Lett.* **2023**, *23* (14), 6637−6644.

(91) Yao, Y.; Liu, Z.; Xie, P.; Huang, Z.; Li, T.; Morris, D.; Finfrock, Z.; Zhou, J.; Jiao, M.; Gao, J.; et al. Computationally aided, entropy-driven synthesis of highly efficient and durable multi-elemental alloy catalysts. *Science Advances* **2020**, *6* (11), No. eaaz0510.

(92) Yeh, J.-W.; Chang, S.-Y.; Hong, Y.-D.; Chen, S.-K.; Lin, S.-J. Anomalous decrease in X-ray diffraction intensities of Cu-Ni-Al-Co-Cr-Fe-Si alloy systems with multi-principal elements. *Mater. Chem. Phys.* **2007**, *103* (1), 41−46.

(93) Li, H.; Lai, J.; Li, Z.; Wang, L. Multi-Sites Electrocatalysis in High-Entropy Alloys. *Adv. Funct. Mater.* **2021**, *31* (47), 2106715.

(94) Liu, Z.; Zhao, Z.; Peng, B.; Duan, X.; Huang, Y. Beyond Extended Surfaces: Understanding the Oxygen Reduction Reaction on Nanocatalysts. *J. Am. Chem. Soc.* **2020**, *142* (42), 17812−17827.

(95) Li, C.; Tan, H.; Lin, J.; Luo, X.; Wang, S.; You, J.; Kang, Y.-M.; Bando, Y.; Yamauchi, Y.; Kim, J. Emerging Pt-based electrocatalysts with highly open nanoarchitectures for boosting oxygen reduction reaction. *Nano Today* **2018**, *21*, 91−105.

(96) Yao, N.; Jia, H.; Zhu, J.; Shi, Z.; Cong, H.; Ge, J.; Luo, W. Atomically dispersed Ru oxide catalyst with lattice oxygen participation for efficient acidic water oxidation. *Chem.* **2023**, *9* (7), 1882−1896.

(97) She, L.; Zhao, G.; Ma, T.; Chen, J.; Sun, W.; Pan, H. On the Durability of Iridium-Based Electrocatalysts toward the Oxygen Evolution Reaction under Acid Environment. *Adv. Funct. Mater.* **2022**, *32* (5), 2108465.

(98) Qin, R.; Chen, G.; Feng, X.; Weng, J.; Han, Y. Ru/Ir-Based Electrocatalysts for Oxygen Evolution Reaction in Acidic Conditions: From Mechanisms, Optimizations to Challenges. *Advanced Science* **2024**, *11* (21), 2309364.

(99) Tao, L.; Sun, M.; Zhou, Y.; Luo, M.; Lv, F.; Li, M.; Zhang, Q.; Gu, L.; Huang, B.; Guo, S. A General Synthetic Method for High-Entropy Alloy Subnanometer Ribbons. *J. Am. Chem. Soc.* **2022**, *144* (23), 10582−10590.

(100) Tian, J.; Rao, Y.; Shi, W.; Yang, J.; Ning, W.; Li, H.; Yao, Y.; Zhou, H.; Guo, S. Sabatier Relations in Electrocatalysts Based on High-entropy Alloys with Wide-distributed d-band Centers for Li-O$_2$ Batteries. *Angew. Chem., Int. Ed.* **2023**, *62* (44), No. e202310894.

(101) Wang, X.; Dong, Q.; Qiao, H.; Huang, Z.; Saray, M. T.; Zhong, G.; Lin, Z.; Cui, M.; Brozena, A.; Hong, M.; et al. Continuous Synthesis of Hollow High-Entropy Nanoparticles for Energy and Catalysis Applications. *Adv. Mater.* **2020**, *32* (46), 2002853.

(102) Zhang, P.; Hui, X.; Nie, Y.; Wang, R.; Wang, C.; Zhang, Z.; Yin, L. New Conceptual Catalyst on Spatial High-Entropy Alloy Heterostructures for High-Performance Li-O$_2$ Batteries. *Small* **2023**, *19* (15), 2206742.

(103) Sun, L.; Yuwono, J. A.; Zhang, S.; Chen, B.; Li, G.; Jin, H.; Johannessen, B.; Mao, J.; Zhang, C.; Zubair, M.; et al. High Entropy Alloys Enable Durable and Efficient Lithium-Mediated CO$_2$ Redox Reactions. *Adv. Mater.* **2024**, *36*, 2401288.

(104) Yi, J.; Deng, Q.; Cheng, H.; Zhu, D.; Zhang, K.; Yang, Y. Unique Hierarchically Structured High-Entropy Alloys with Multiple Adsorption Sites for Rechargeable Li-CO$_2$ Batteries with High Capacity. *Small* **2024**, *20*, 2401146.

(105) Choi, S.; Kwon, J.; Park, C.; Park, K.; Park, H. B.; Paik, U.; Song, T. FeCoNiCuIr High-Entropy Alloy Catalysts for Hydrogen Evolution Reactions with Improved Desorption Behavior by Tuning Antibonding Orbital Filling. *Energy Fuels* **2023**, *37* (23), 18128−18136.

(106) Zhang, Q.; Lian, K.; Liu, Q.; Qi, G.; Zhang, S.; Luo, J.; Liu, X. High entropy alloy nanoparticles as efficient catalysts for alkaline overall seawater splitting and Zn-air batteries. *J. Colloid Interface Sci.* **2023**, *646*, 844−854.

(107) Jin, Z.; Lyu, J.; Zhao, Y.-L.; Li, H.; Lin, X.; Xie, G.; Liu, X.; Kai, J.-J.; Qiu, H.-J. Rugged High-Entropy Alloy Nanowires with in

Situ Formed Surface Spinel Oxide As Highly Stable Electrocatalyst in Zn-Air Batteries. *ACS Materials Letters* **2020**, *2* (12), 1698−1706.

(108) He, R.; Yang, L.; Zhang, Y.; Jiang, D.; Lee, S.; Horta, S.; Liang, Z.; Lu, X.; Ostovari Moghaddam, A.; Li, J.; et al. A 3d-4d-5d High Entropy Alloy as a Bifunctional Oxygen Catalyst for Robust Aqueous Zinc-Air Batteries. *Adv. Mater.* **2023**, *35* (46), 2303719.

(109) Gao, L.; Zhong, X.; Li, Z.; Hu, J.; Cui, S.; Wang, X.; Xu, B. A multi-layer reduced graphene oxide catalyst encapsulating a high-entropy alloy for rechargeable zinc-air batteries. *Chem. Commun.* **2024**, *60* (10), 1269−1272.

(110) Cao, X.; Gao, Y.; Wang, Z.; Zeng, H.; Song, Y.; Tang, S.; Luo, L.; Gong, S. FeNiCrCoMn High-Entropy Alloy Nanoparticles Loaded on Carbon Nanotubes as Bifunctional Oxygen Catalysts for Rechargeable Zinc-Air Batteries. *ACS Appl. Mater. Interfaces* **2023**, *15* (27), 32365−32375.

(111) Wu, D.-H.; Ul Haq, M.; Zhang, L.; Feng, J.-J.; Yang, F.; Wang, A.-J. Noble metal-free FeCoNiMnV high entropy alloy anchored on N-doped carbon nanotubes with prominent activity and durability for oxygen reduction and zinc-air batteries. *J. Colloid Interface Sci.* **2024**, *662*, 149−159.

(112) He, R.; Yang, L.; Zhang, Y.; Wang, X.; Lee, S.; Zhang, T.; Li, L.; Liang, Z.; Chen, J.; Li, J.; et al. A CrMnFeCoNi high entropy alloy boosting oxygen evolution/reduction reactions and zinc-air battery performance. *Energy Storage Materials* **2023**, *58*, 287−298.

(113) Yao, Y.; Li, Z.; Dou, Y.; Jiang, T.; Zou, J.; Lim, S. Y.; Norby, P.; Stamate, E.; Jensen, J. O.; Zhang, W. High entropy alloy nanoparticles encapsulated in graphitised hollow carbon tubes for oxygen reduction electrocatalysis. *Dalton Transactions* **2023**, *52* (13), 4142−4151.

(114) Madan, C.; Jha, S. R.; Katiyar, N. K.; Singh, A.; Mitra, R.; Tiwary, C. S.; Biswas, K.; Halder, A. Understanding the evolution of catalytically active multi-metal sites in a bifunctional high-entropy alloy electrocatalyst for zinc-air battery application. *Energy Advances* **2023**, *2* (12), 2055−2068.

(115) Fang, G.; Gao, J.; Lv, J.; Jia, H.; Li, H.; Liu, W.; Xie, G.; Chen, Z.; Huang, Y.; Yuan, Q.; et al. Multi-component nanoporous alloy/(oxy)hydroxide for bifunctional oxygen electrocatalysis and rechargeable Zn-air batteries. *Applied Catalysis B: Environmental* **2020**, *268*, 118431.

(116) Jin, Z.; Zhou, X.; Hu, Y.; Tang, X.; Hu, K.; Reddy, K. M.; Lin, X.; Qiu, H.-J. A fourteen-component high-entropy alloy@oxide bifunctional electrocatalyst with a record-low ΔE of 0.61 V for highly reversible Zn-air batteries. *Chemical Science* **2022**, *13* (41), 12056−12064.

(117) Yu, T.; Zhang, Y.; Hu, Y.; Hu, K.; Lin, X.; Xie, G.; Liu, X.; Reddy, K. M.; Ito, Y.; Qiu, H.-J. Twelve-Component Free-Standing Nanoporous High-Entropy Alloys for Multifunctional Electrocatalysis. *ACS Materials Letters* **2022**, *4* (1), 181−189.